Some mechanistic underpinnings of molecular adaptations of SARS-COV-2 spike protein by integrating candidate adaptive polymorphisms with protein dynamics

Nicholas J. Ose[1], Paul Campitelli[1], Tushar Modi[1], I. Can Kazan[1], Sudhir Kumar[2,3,4,*] and S. Banu Ozkan[1,*]

[1]Department of Physics and Center for Biological Physics, Arizona State University, Tempe, Arizona, United States of America

[2]Institute for Genomics and Evolutionary Medicine, Temple University, Philadelphia, Pennsylvania, United States of America

[3]Department of Biology, Temple University, Philadelphia, Pennsylvania, United States of America

[4]Center for Genomic Medicine Research, King Abdulaziz University, Jeddah, Saudi Arabia

* s.kumar@temple.edu (SK); * Banu.Ozkan@asu.edu (SBO)

Abstract

We integrate evolutionary predictions based on the neutral theory of molecular evolution with protein dynamics to generate mechanistic insight into the molecular adaptations of the SARS-COV-2 Spike (S) protein. With this approach, we first identified Candidate Adaptive Polymorphisms (CAPs) of the SARS-CoV-2 Spike protein and assessed the impact of these CAPs through dynamics analysis. Not only have we found that CAPs frequently overlap with well-known functional sites, but also, using several different dynamics-based metrics, we reveal the critical allosteric interplay between SARS-CoV-2 CAPs and the S protein binding sites with the human ACE2 (hACE2) protein. CAPs interact far differently with the hACE2 binding site residues in the open conformation of the S protein compared to the closed form. In particular, the CAP sites control the dynamics of binding residues in the open state, suggesting an allosteric control of hACE2 binding. We also explored the characteristic mutations of different SARS-CoV-2 strains to find dynamic hallmarks and potential effects of future mutations. Our analyses reveal that Delta strain-specific variants have non-additive (i.e., epistatic) interactions with CAP sites, whereas the less pathogenic Omicron strains have mostly additive mutations. Finally, our dynamics-based analysis suggests that the novel mutations observed in the Omicron strain epistatically interact with the CAP sites to help escape antibody binding.

Introduction

Since 2019, the evolution of SARS-CoV-2 in humans has been characterized by the spread of mutations, many notably found within the Spike (S) glycoprotein. The S protein is directly related to the human immune response to COVID-19 and, as such, has been one of the most studied and targeted proteins in SARS-CoV-2 research (Shang et al. 2020; Harvey, Carabelli, Jackson, Gupta, Thomson, Harrison, Ludden, Reeve, Rambaut, Consortium, et al. 2021; Jackson et al. 2022; Carabelli et al. 2023; Markov et al. 2023). Subsequently, research into the biophysical properties and mutational patterns associated with S protein

41 evolution not only remains critical to understanding the pandemic but also emerges as a useful system to
42 understand the mechanics of molecular adaptation within viruses.

43 For successful infection of a human host, the S glycoprotein of SARS-CoV-2 binds to the human ACE2
44 (hACE2) receptor through its receptor-binding domain (RBD). Evidence indicates that fine-tuning S protein
45 interactions with hACE2 significantly affects viral reproduction (Rehman et al. 2020; Saputri et al. 2020;
46 Rochman et al. 2021). Previous evolutionary studies show a complex network of interactions among
47 mutated residues (Changeux and Edelstein 2005; Doshi et al. 2016; O'Rourke et al. 2016; Mishra and
48 Jernigan 2018). Therefore, there has been a vast effort to uncover which mutations are important steps
49 of adaptation for the S protein (Cagliani et al. 2020; Damas et al. 2020; Singh and Yi 2021; Kistler et al.
50 2022; Maher et al. 2022; Neher 2022). In particular, a significant aspect of many such studies was a focus
51 on understanding adaptive mutations of SARS-CoV-2 that contributed to the leap to human hosts (Cagliani
52 et al. 2020; Damas et al. 2020; Singh and Yi 2021; Starr, Zepeda, et al. 2022). This is because SARS-CoV-2
53 has continuously mutated since its early detection (Kistler et al. 2022), causing the emergence of CDC-
54 designated "variants of concern" (VOCs) that may be driven by an accelerated substitution rate may (Tay
55 et al. 2022).

56 Predicting how new mutations impact the biophysical properties of the S protein remains a challenge, let
57 alone explaining their complex interactions with one another and how they might affect hACE2 binding;
58 many factors affect hACE2 interactions. Binding affinity with hACE2 can be enhanced directly through
59 stronger receptor interactions or mediated through changes in RBD opening (Natália Teruel et al. 2021a;
60 Zhang et al. 2021; Díaz-Salinas et al. 2022). The RBD exhibits both 'closed' and 'open' conformational
61 states. In the closed state, the RBD is shielded from receptor binding. In the open state, the RBD is
62 accessible for hACE2 binding (Kirchdoerfer et al. 2016; Gur et al. 2020; Henderson et al. 2020; Hoffmann
63 et al. 2020a). While some mutations may affect the transition between these states (Henderson et al.
64 2020; Yurkovetskiy et al. 2020; Gobeil, Janowska, McDowell, Mansouri, Parks, Manne, et al. 2021; Sztain

65 et al. 2021; Zhang et al. 2021; Shoemark et al. 2022), other mutations may allosterically regulate RBD
66 openings through Furin cleavage site (residue ID range: 681-695) interactions to regulate hACE2 binding
67 (Deng et al. 2021; Gobeil, Janowska, McDowell, Mansouri, Parks, Stalls, et al. 2021; Khan et al. 2021;
68 Laiton-Donato et al. 2021).

69 Moreover, as new mutations accumulate, culminating in the emergence of a new VOC, these mutations
70 must occur on varied sequence backgrounds containing neutral, nearly-neutral, and adaptive mutations.
71 While many studies have explored the impacts of individual mutations, VOCs result in a substantial
72 difference in protein function as compared to their individual effects (Moulana et al. 2022a; Starr,
73 Greaney, Hannon, et al. 2022; Moulana et al. 2023; Witte et al. 2023). Here we integrate an evolutionary
74 approach with protein dynamics analysis to address the fundamental mechanisms of mutations dictating
75 VOCs and the impact of their epistatic interaction on the function of the S protein. Many earlier studies
76 have combined phylogeny and evolutionary theory to identify adaptive mutations and analyze how the
77 viral sequence has changed over time (Frost et al. 2018; Boni et al. 2020; Cagliani et al. 2020; Damas et al.
78 2020; Tang et al. 2020). Similarly, we first use a well-established Evolutionary Probability (EP) approach
79 (Liu et al. 2016) that utilizes phylogenetic trees in combination with the neutral theory of molecular
80 evolution to determine Candidate Adaptive Polymorphisms (CAPs) using the early Wuhan sequence as a
81 variant. CAPs are substitutions in SARS-CoV-2 that are rarely observed in other closely related sequences
82 (Figure 1A), which implies a degree of functional importance and makes them candidates for adaptation
83 (Liu et al. 2016). Adaptation in this case means a virus which can successfully infect human hosts. As CAPs
84 are unexpected polymorphisms under neutral theory, their existence implies a non-neutral effect. This
85 can come in the form of functional changes (liu et al. 2016) or compensation for functional changes (Ose
86 et al. 2022). Therefore, we suspect that these CAPs may be partially responsible for the functional change
87 allowing the infection of human hosts. In support of this method, we find an overlap between our list of
88 sites containing CAPs and putative adaptive sites identified by others (Cagliani et al. 2020; Singh and Yi

89 2021; Kistler et al. 2022; Starr, Zepeda, et al. 2022). Second, we use a suite of computational tools to
90 analyze how CAPs that arose in the early and late phases of the COVID-19 pandemic modulate the
91 dynamics of the S protein. We also explore the complex interactions between these sets of CAPs to gain
92 mechanistic insight into the behavior of molecular adaptation involving the S protein. In particular, we
93 focused on how mutations modulate protein dynamics, as we and others have previously found that
94 rather than changing a protein's structure solely, mutations modulate conformational dynamics leading
95 to changes in biophysical properties such as stability, flexibility, and allosteric dynamic coupling, any of
96 which may affect protein binding (Swint-Kruse et al. 1998; Keskin et al. 2000; Bhabha et al. 2013; Nussinov,
97 R., Tsai, C.-J 2013; Campbell, E. et al. 2016; Ma and Nussinov 2016: 201; Saavedra et al. 2018; Kuzmanic
98 et al. 2020).

99 With this evolutionary-dynamics unified approach, we aim to answer the following questions about VOCs:
100 Are all the mutations in VOCs adaptive in nature? Are they coupled to one another or provide some
101 measure of biophysical, dynamical, or mechanical epistasis? While many of these mutations are found
102 within the RBD domain, numerous others are located distal to this region; hence, we aim to investigate
103 the functional roles of distal mutations, particularly from a protein dynamics perspective. Our integrated
104 analysis revealed that protein dynamics play a significant role in the evolution of the S protein. The
105 flexibility of sites within the S protein shows a strong, direct correlation with substitution rate, and newly
106 evolving CAPS are mostly additive mutations that modulate the dynamics of the hACE2 binding site. Yet
107 other CAPs, 346R, 486F, and 498Q, show highly epistatic (i.e., non-additive) modulation of the hACE2
108 binding site and provide immune escape benefits.

109

110 **Results and Discussions**

111 **Candidate Adaptive mutations in the Spike protein are recognized via Evolutionary Probabilities.**

112 SARS-CoV-2 is part of a family of coronaviruses, many of which infect mainly animals and are less capable
113 of infecting humans (Dicken et al. 2021). Therefore, to identify the most likely mutations responsible for
114 the infection of human hosts (i.e., putative adaptive mutations for humans), we estimated the (neutral)
115 evolutionary probability (EP) scores of mutations found within the S protein (Liu et al. 2016). EP scores of
116 the amino acid variants of the S protein were obtained using a Maximum Likelihood phylogeny (Kumar et
117 al. 2018) built from 19 orthologous coronavirus sequences. Sequences were selected by examining
118 available non-human sequences with a sequence identity of 70% or above to the human SARS CoV-2's S
119 protein sequence. This cutoff allows for divergence over evolutionary history such that each amino acid
120 position had ample time to experience purifying selection, whilst limiting ourselves to closely related
121 coronaviruses. (Figure 1A). The likelihood of finding a particular amino acid in the sequence is then
122 determined using a Bayesian framework, with calculations carried out by MEGA X software (Kumar et al.
123 2018). As apparent in the name, EP scores obtained for the amino acids in the sequence provide
124 information regarding the likelihood of finding them at their position, given the history of the sequence.
125 Amino acid residues receiving low EP scores (<0.05) at a position are less likely to be found in a given
126 position within the sequence because they are non-neutral. Generally, positions with low EP amino acids
127 are far less common than those containing mutations with high EP, a trend also realized in the CoV-2 S
128 protein (Figure 1B).

129 Of particular interest is an observed evolutionary change where an amino acid with high EP is replaced by
130 an amino acid residue with low EP. While amino acids with low EP should be harmful or deleterious to
131 viral fitness due to functional disruption or change, fixation of a low EP amino acid at a position suggests
132 an underlying mechanism for natural selection to operate. These fixed, low EP mutations are called
133 candidate adaptive polymorphisms (CAPs) as they are predicted to alter protein function, and adaptive
134 pressures may drive their prevalence (Patel et al. 2018). Indeed, there is an overlap between these CAPs
135 and the mutations suggested by other methods to be adaptive for the S protein (Cagliani et al. 2020; Singh

136 and Yi 2021; Kistler et al. 2022; Starr, Zepeda, et al. 2022). Within these studies, sites 478, 486, 498, and
137 681 have been implicated in SARS-CoV-2 evolution, leaving the remaining 11 CAPs as undiscovered
138 candidate sites for adaptation.

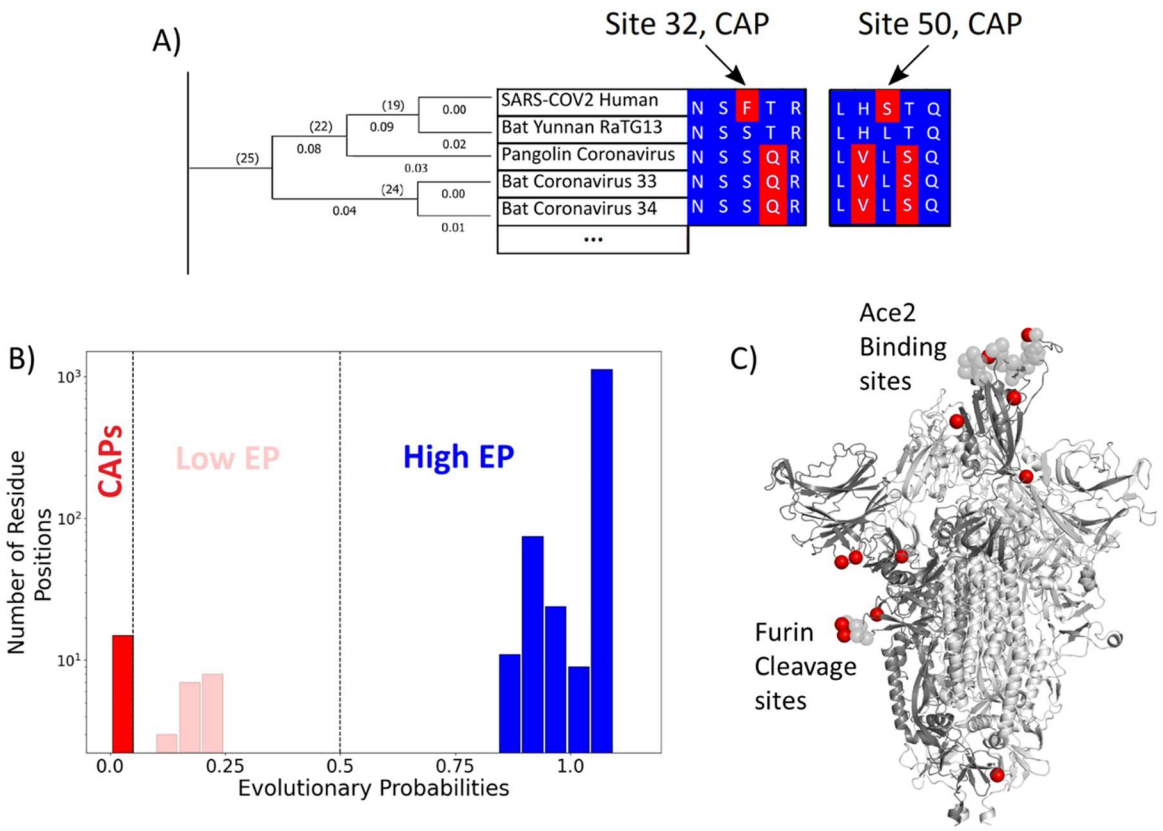

139

140 **Figure 1.** (A) The evolutionary probabilities (EP) of each amino acid in the S protein sequence are
141 calculated by taking the multiple sequence alignment of the S proteins through their evolutionary tree
142 and using Bayesian inferences to determine the likelihood of finding a particular residue at a particular
143 location within a given sequence. Simply, if the residue is found at a location 'x' in closely related
144 sequences, it will have a higher EP at location 'x' in the target sequence. Residues with an EP <0.05 in the
145 target sequence are CAPs (Red). CAPs are found at sites 32, 50, 218, 346, 372, 478, 486, 498, 519, 604,
146 681, 682, 683, 684, and 1125. (B) The distribution of EP scores of the wild-type residues in the S protein.
147 Here, lower EP scores are shown in red, and higher EP scores in blue. While the vast majority of the wild-
148 type (reference) protein consists of high EP residues, a few residues have low EP. (C) The CAPs are also
149 highlighted as red spheres in the open configuration of the S protein, with the open chain in a darker

150 shade. We observe that a majority of the CAP positions reside at the receptor binding domain (RBD) and
151 the Furin cleavage site (676-689; (Wrobel et al. 2020)) shown as transparent light gray spheres.

152 Interestingly, most of the CAP residues are at functionally critical sites, including the receptor binding
153 domain (RBD) and the Furin cleavage site (Figure 1C). As mentioned earlier, the RBD plays a key role in
154 initiating the infection of a healthy cell by binding with the host organism's ACE2 protein. Before ACE2
155 binding, one chain of the homotrimer comprising the S protein must open to expose the RBD (Kirchdoerfer
156 et al. 2016; Henderson et al. 2020; Hoffmann et al. 2020a; Sztain et al. 2021). The Furin cleavage site plays
157 a key role in the opening process as the binding of host cell protease Furin aids in the cleavage of the S
158 protein into two domains: S1 and S2 (Wrobel et al. 2020: 13). Another host cell protease, TMPRSS2,
159 facilitates viral attachment to the surface of target cells upon binding either to sites Arg815/Ser816, or
160 Arg685/Ser686 which overlap with the furin cleavage site 676-689, further emphasizing the importance
161 of this area (Hoffmann et al. 2020b; Fraser et al. 2022). Similar cleavage sites have been found in related
162 coronaviruses, including HKU1 and Middle East respiratory syndrome coronavirus (MERS-CoV), which
163 infects humans (Chan et al. 2008: 1; Millet and Whittaker 2014; Millet and Whittaker 2015), and the
164 acquisition of similar cleavage sites is associated with increased pathogenicity in other viruses such as the
165 influenza virus (Steinhauer 1999). Interestingly, however, CAPs do not display such an overwhelming
166 tendency to occur at well-known critical sites within human proteins studied with similar methods (Ose,
167 Campitelli, et al. 2022), yet mutations at those sites are associated with disease, indicating their critical
168 role in inducing functional change. Therefore, the identified CAPs in the S protein, which are signs of
169 recent evolution, can provide mechanistic insights regarding the molecular adaptation of the virus. In
170 particular, we aimed to analyze how these CAP positions in the S protein modulate the interaction with
171 hACE2 using our protein dynamics-based analysis (Gerek and Ozkan 2011; Nevin Gerek, Z., Kumar, S., Banu
172 Ozkan, S. 2013; Larrimore et al. 2017; Kumar, A., Glembo, T.J., Ozkan, S.B. 2015b).

173

174 **Asymmetry in communications among the network of interactions in Spike describes how CAPs regulate**
175 **the dynamics of the Spike protein.**

176 A mutation at a given amino acid position inevitably not only alters local interactions, but this change
177 cascades through the residue-residue interaction network, which gives rise to a variation in native
178 ensemble dynamics to modulate function (Dror et al. 2012; Labbadia and Morimoto 2015; Sekhar and Kay
179 2019; Campitelli et al.). Many groups have already examined the conformational dynamics of the spike
180 protein using normal mode analysis to explore mutation sites and interactions with different receptors
181 (Zhou et al. 2020; Majumder et al. 2021; Natália Teruel et al. 2021b; Natalia Teruel et al. 2021; Verkhivker
182 2022). However, our study will focus mainly on the role of CAPs, of which F486 and Q498 have already
183 been identified through Perturbation Response Scanning (PRS) as potential allosteric sites (Verkhivker
184 2022). Thus, we analyze the internal dynamics of the system to understand the functional role of CAPs in
185 S proteins. This analysis allows us to gain a mechanistic understanding of the relationship between CAP
186 mutations and biophysical outcomes (Natália Teruel et al. 2021a). First, we implement the Dynamic
187 Coupling Index (DCI) approach to study long-distance coupling between the CAPs and the hACE2 binding
188 sites emerging from the 3D network of interactions across the S protein system. DCI calculation combines
189 Perturbation Response Scanning and Linear Response Theory to capture the strength of a displacement
190 response for position *i* upon perturbation of position *j*, relative to the average fluctuation response of
191 position *i* to all other positions in the protein. It represents the strength of dynamic coupling between
192 positions *i* and *j* upon perturbation to *j* (Larrimore et al. 2017; Kumar, A., Glembo, T.J., Ozkan, S.B. 2015b).

193 Further, asymmetry can be captured in the DCI values, as dynamic coupling is not necessarily symmetric
194 due to an anisotropic interaction network. That is, each amino acid has a set of positions to which it is
195 highly coupled, and this anisotropy in connections gives rise to unique differences in coupling between a
196 given *i, j* pair of amino acids which do not have direct interactions. By calculating the coupling of the hACE2
197 binding interface in the RBD with respect to the CAP residue positions and vice versa, we can generate

198 DCI_{asym} (Figure 2A) as the difference between the normalized displacement response of position *j* upon a
199 perturbation to position *i* (DCI_{ij}) and the normalized displacement response of position *i* upon a
200 perturbation to position *j* (DCI_{ji}) (See Methods). If the DCI_{asym} values significantly differ from zero, it shows
201 asymmetry in coupling and presents a cause-effect relationship between the *i, j* pair in terms of
202 force/signal propagation. This metric has been used previously in a variety of systems to analyze the
203 unique behavior of positions within a protein and a given position's propensity to effect biophysical
204 changes upon mutation, particularly at long distances (Modi and Ozkan 2018; Campitelli and Ozkan 2020;
205 Kolbaba-Kartchner et al. 2021; Ose, Butler, et al. 2022; Kazan et al. 2023; Campitelli et al. 2020b).

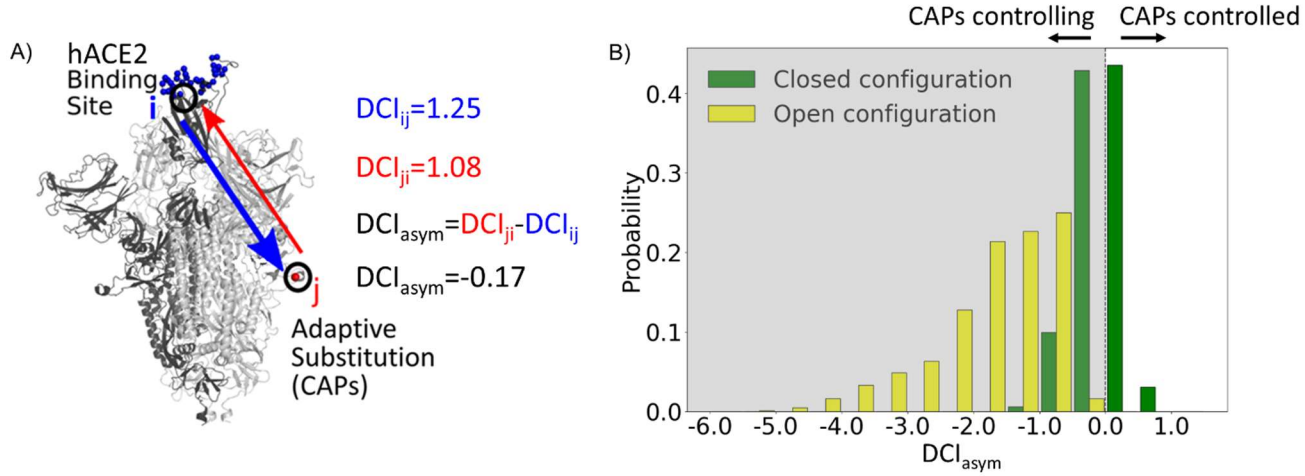

206

207 **Figure 2.** (A) Schematic representation of DCI_{asym}. (B) DCI_{asym} of CAP residue positions with the binding
208 interface of RBD in the open chain. Residues in the closed chains with a low EP amino acid in the reference
209 sequence dominate the binding site interface of RBD in the open chain. There is a significant difference
210 between the asymmetry profiles of the closed (M = -0.06, SD = 0.33) and open (M = -1.68, SD = 0.89)
211 conformations ($p < .001$).
212

213 Recent work from our group has shown an enhancement in cross-chain communication within the main
214 protease of SARS COV-2 compared to SARS COV-1 (Campitelli et al. 2022). Furthermore, previous studies
215 have shown that allosteric inter-chain communication is important to S protein function (Zhou et al. 2020;

216 Spinello et al. 2021; Tan et al. 2022; Xue et al. 2022). In support of these findings, we observe through
217 DCI_{asym} that when the S protein is in its pre-fusion conformation with one chain open, the CAPs in the
218 closed chains have negative coupling asymmetry with respect to the hACE2 binding site interface in the
219 RBD-open chain. This indicates an allosteric control where the hACE2 binding site is dominated by the
220 dynamics of the CAPs in closed chains (Figure 2B, yellow bars). As this open state RBD is critical for the
221 viral infection of host cells (Kirchdoerfer et al. 2016), our results suggest that this type of closed-to-open
222 cross-chain interaction is important for viral proliferation. Our prior studies on DCI_{asym} show a similar trend
223 in Lactose Inhibitor (LacI), a protein with a functional role in gene expression through binding DNA. The
224 allosteric mutations (i.e., mutations on the sites that are far from the DNA binding sites) that alter DNA
225 binding affinity not only exhibited unique asymmetry profiles with the DNA binding sites of LacI, but also
226 regulated the dynamics of these binding sites (Campitelli et al. 2020b).

227 Similarly, it is possible that mutations to such residue positions within the S protein can be used to regulate
228 the dynamics of the hACE2 bindings sites of the open RBD state. We, therefore, propose that the residue
229 positions with CAP substitutions hold the potential for mutations in the spike sequence which can alter
230 the opening and closing dynamics of the RBD domain. This hypothesis is further supported by many
231 mutations already observed at these residue positions which alter the infection rate (Brister et al. 2015).
232 Interestingly, residues responsible for extremely low asymmetry values (< -4) lie overwhelmingly in the
233 region 476–486. These same residues were suggested to stabilize S protein dynamics and prime it for host
234 Furin proteolysis (Raghuvamsi et al. 2021).

235 Moreover, as a control, we performed the same analysis on the S protein with the RBD domains of all
236 chains in the closed configuration. In this case, we observed that the DCI_{asym} of the CAPs residue positions
237 with respect to the hACE2 interface in the other chains yields a largely symmetric distribution about 0
238 (Figure 2B, green bars). This verifies that the asymmetry in the coupling of CAPs with the exposed binding

239 site interface in pre-fusion configuration results from one of the RBDs opening up and further suggests
240 the allosteric role played by CAPs in locking the S protein in the RBD open state.

241

242 **Dynamics analysis shows that rigid sites tend to be more highly conserved than flexible sites.**

243 CAPs represent important S protein amino acid changes between related coronaviruses across multiple
244 species and the Wuhan-Hu-1 reference sequence (MN908947). Since SARS-CoV-2 first spread to humans,
245 it has continued to mutate and evolve rapidly, particularly regarding the S protein (Amicone et al. 2022;
246 Liu et al. 2022; Tay et al. 2022). Just as mutations leading to the Wuhan strain caused an increase in binding
247 affinity to hACE2, continued evolution in human hosts has resulted in further altered binding affinities as
248 well as different phenotypic outcomes for those infected (Ali et al. 2021; Barton et al. 2021; Ozono et al.
249 2021).

250 We explore whether protein dynamics has played a role in the selection of mutational sites during the
251 evolution of the S protein since 2019. Our previous work has indicated that rate of evolution per positional
252 site exhibits a positive correlation with positional flexibility; generally, positions that exhibit higher
253 flexibility are also sites that experience a higher number of amino acid substitutions (Liu and Bahar 2012;
254 Maguid et al. 2008; Maguid et al. 2006; Mikulska-Ruminska et al. 2019; Nevin Gerek, Z., Kumar, S., Banu
255 Ozkan, S. 2013). To confirm these findings for the evolution of the S protein using the sequenced variants
256 of infected humans, we examine the flexibility of the S protein, an analysis conducted in other studies
257 which resulted in several important findings (Nguyen et al. 2020; Socher et al. 2021; Natália Teruel et al.
258 2021b; Natalia Teruel et al. 2021; Pipitò et al. 2022; Verkhivker 2022; Abduljalil et al. 2023). For example,
259 Teruel et al. (2021) used their Elastic Network Contact Model to find how certain highly observed
260 mutations make the open state more rigid and the closed state more flexible. For our own flexibility
261 analysis, we measure the site-specific amino acid flexibility using the Dynamic Flexibility Index (DFI). Using

262 the same mathematical foundation as DCI, DFI evaluates each position's displacement response to
263 random force perturbations at other locations in the protein (Gerek and Ozkan 2011; Nevin Gerek, Z.,
264 Kumar, S., Banu Ozkan, S. 2013), and it can be considered a measure of a given position's ability to explore
265 its local conformational space. We found that the covid-19 S protein shows the expected high correlation
266 between the occurrence of mutations and site flexibility (Figure 3) when we compare %DFI (DFI ranked
267 by percentile) to the average number of variants per position found within a given %DFI bin. Previous
268 studies have indicated that rigid residues are critical for functional dynamics, thus more likely to impact
269 function if mutated and, generally, can lead to a loss of function and thus more conserved (Kim, H. et al.
270 2015; Butler et al. 2018; Modi, Risso, et al. 2021; Modi, Campitelli, et al. 2021; Kazan et al. 2022; Ose,
271 Butler, et al. 2022; Stevens et al. 2022; Campitelli et al. 2020a; Kumar, A., Glembo, T.J., Ozkan, S.B. 2015b).
272 This analysis also agrees with these previous studies and highlights the power of negative selection, in line
273 with the neutral theory of molecular evolution, stating that deleterious mutations (i.e., those on the rigid
274 positions) should be eliminated and therefore not observed (Kimura, Motoo 1983).

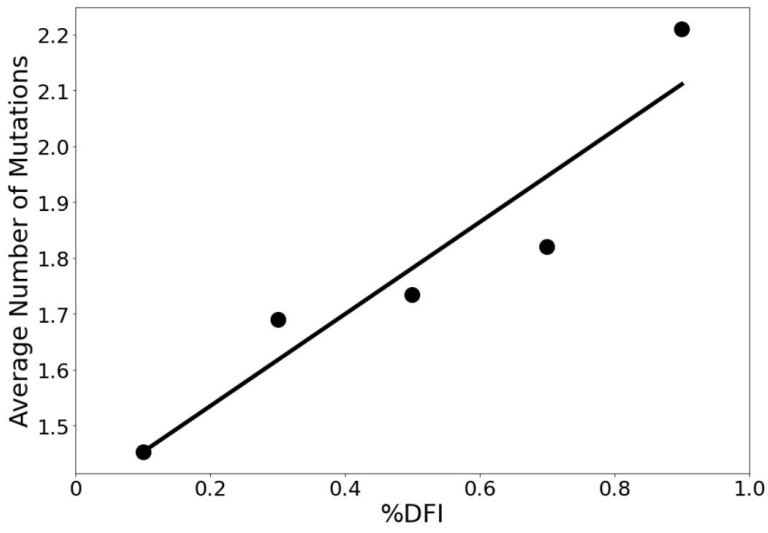

275

276 **Figure 3**. The average number of variants observed among residues of different flexibility. Residues were
277 sorted into one of five bins based on flexibility. After that, the average number of variants for residues
278 within that bin was calculated. Here, the number of variants is defined as the number of different amino

279 acid varieties found at that site. Mutational data was calculated across approximately 24,000 SARS-CoV-
280 2 S protein sequences from the NCBI Datasets Project (Brister et al. 2015). Residue flexibility, as reported
281 here via %DFI, was computed using PDB id 6vsb from the Protein DataBank (Berman, H.M. et al. 2000).
282 More rigid residues tend to have fewer variants. (r = 0.94).

283 Continued mutations within human hosts have resulted in a multitude of variants. Indeed, by fitting
284 various molecular clock models to genome sequence data, VOC emergence is punctuated by an episodic
285 period of rapid evolution, with a substitution rate of up to 4-fold greater than the background substitution
286 rate (Kumar et al. 2021; Tay et al. 2022). With such an aggressive evolutionary rate, we are finding VOCs
287 to consist of a number of different characteristic mutations, almost all of which are CAPs. Sequence
288 differences between the various VOCs used in this paper can be found in Supplementary Figure S1.

289 To explore the dynamic effects of the evolution of the Spike in humans, we examine asymmetry with these
290 new potentially adaptive sites, namely the low EP (CAP) characteristic mutation sites observed in the Delta
291 variant, the widely dominant variant from December 2021 to January 2022 (Thye et al. 2021), and the
292 Omicron variant, a highly transmissible variant whose lineages have remained dominant since January
293 2022) (Kim et al. 2021) (Figure 4). This analysis revealed a mechanism similar to that for the CAPs in the
294 reference protein (Figure 2), as the open-chain binding interface is also allosterically controlled by these
295 potentially new adaptive sites. Regarding this, we see that the asymmetry is much more pronounced in
296 observed mutations of Omicron variants suggesting that these new mutations have a stronger power in
297 controlling the dynamics of open chain hACE2 binding interface compared to those observed in Delta
298 variants. We surmise that the difference in virulence and infection rates between Omicron and Delta
299 (Earnest et al. 2022; Bager et al. 2021; Sheikh et al. 2021; Twohig et al. 2022;(Houhamdi et al. 2022; Menni
300 et al. 2022) might be due to these specific CAPs within each variant and their differences in allosterically
301 controlling the dynamics of open RBD binding sites as also observed in the DCI_{asym} analysis of the Wuhan
302 variant in Figure 2.

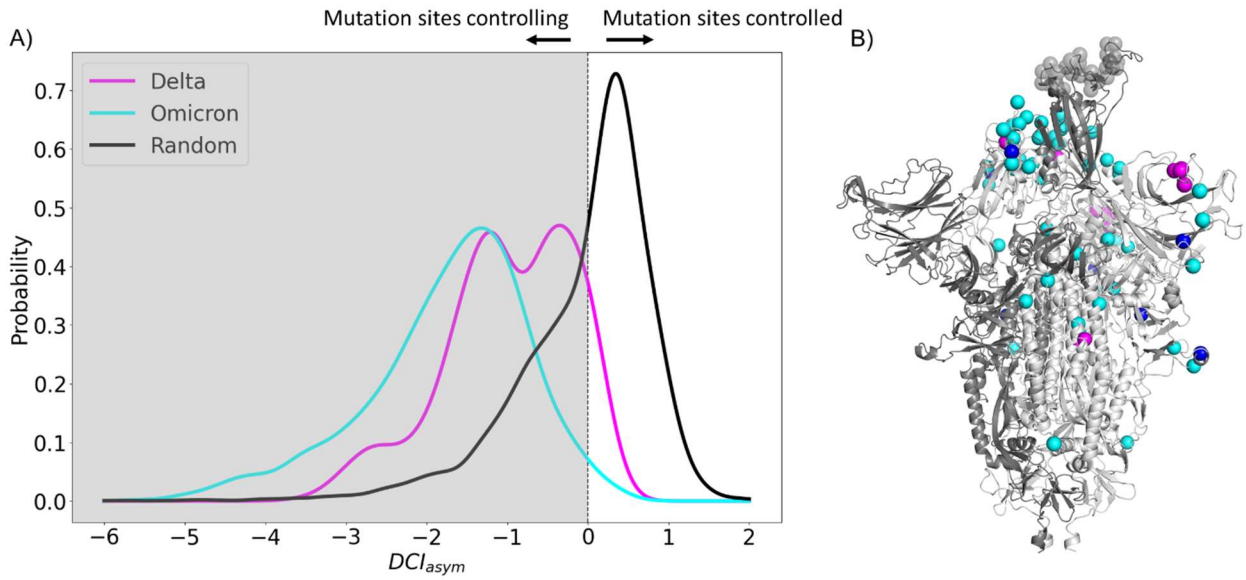

Figure 4. (A) DCI_{asym} with low EP characteristic mutation sites of Delta or Omicron strains in the closed chains and the binding interface of RBD in the open chain. Delta displays a second peak closer to zero, suggesting that Delta mutation sites (M = -0.98, SD = 0.80) have less allosteric control over the hACE2 binding sites than Omicron mutation sites (M = -1.74, SD = 1.00) ($p < .001$). However, both sets of sites have far more control over hACE2 binding sites than expected, based on a random control group (M = 0.03, SD = 0.85) ($p < .001$). (B) S protein structure showing binding interface sites (transparent gray), Delta mutation sites (magenta), Omicron mutation sites (cyan), and sites mutated in both Omicron and Delta (Blue).

Experimental results motivate the use of EpiScore within the SARS-CoV-2 Spike protein.

The fact that the identified CAPs in the reference protein and the more recently evolved CAPs of Delta and Omicron variants both show a high degree of control over the functional sites begs the question: what is the complex interaction between these previous and new CAP sites? Motivated by this concept, we explore the interplay of mutational pairs to understand the effects of the specific amino acid backgrounds associated with these two predominant variants. Some CAP sites in Delta and Omicron have already been considered adaptive (Kemp et al. 2021; Kistler et al. 2022; Maher et al. 2022; Neher 2022).

320 It is well understood that the impact of even a single mutation to a protein sequence can sometimes
321 dramatically alter the biophysical behavior of the system. However, the mechanistic impact of point
322 mutations can only be fully understood when the sequence background upon which it is made is
323 accounted for. This means that, in the case of strains with multiple mutations, the interplay between
324 mutated positions will ultimately impact a protein as an aggregate behavior, where the presence of
325 previous mutations may strongly (or weakly) influence some mutations. This concept of non-additivity is
326 known as epistasis. In fact, studies of evolutionary pathways of mutations have suggested that a majority
327 of the mutations have a second or a higher order epistasis among them (Bershtein et al. 2006). Nature
328 exploits this higher order complex relationship between the mutations to evolve their function.
329 To computationally capture and interpret the pairwise effects of mutations, we have developed an in-
330 house computational tool called EpiScore (Figure 5A). Here, we evaluate how a given position pair *i j* may
331 affect other critical positions *k* of the protein. EpiScore is the relative coupling strength to a position *k*
332 when positions *i* and *j* are perturbed *simultaneously* compared to the average dynamic coupling strength
333 of *i* to *k* and *j* to *k.* EpiScore has previously been used successfully to capture overarching trends in GB1
334 deep mutational scan data as well as specific instances of the development of antibiotic resistance in
335 various enzymatic systems (Campitelli and Ozkan 2020). An EpiScore of 1 indicates perfect coupling
336 additivity, and deviations from this value represent non-additive behavior between position pairs and
337 functionally important sites. Prior EpiScore work has shown a difference in EpiScore between the sites of
338 compensatory and non-compensatory mutations, where both yield distributions with peaks around 1, but
339 non-compensatory mutations show higher deviation in their EpiScore distribution (Ose, Campitelli, et al.
340 2022).

Many studies have confirmed epistasis between residues within the S protein (Moulana et al. 2022a; Starr, Greaney, Hannon, et al. 2022; Moulana et al. 2023; Witte et al. 2023). These epistatic residues can have various effects on hACE2 or antibody binding. Within SARS-CoV-2, here we calculate the EpiScore (Figure 5B) of a set of mutation pairs used by Moulana et al. (Nature comm 2022) and compare our results to quantified epistatic effects determined by the experimental hACE2 binding affinity of "first-order" single mutation variants compared to "second-order" mutation pairs. Our EpiScore results and the experimentally determined epistasis both captured highly epistatic behavior among residues 493, 496, 498, 501, and 505, as well as a lack of epistatic behavior for residues 339, 371, 373, and 375, however EpiScore generally showed higher epistasis values than experiment for residues 417, 440, 446, 477, 478, and 484.

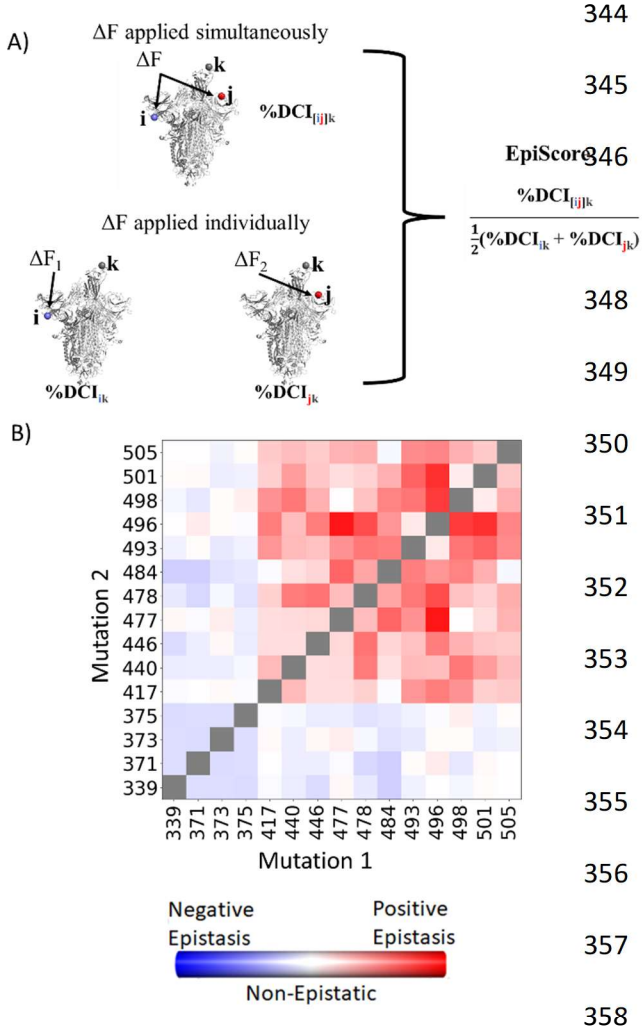

Figure 5. (A) Schematic representation of cross-chain EpiScore, describing i, j, in chain B and C respectively and its impact in RBD binding position k in the open RBD conformer chain A. (B) Colors indicate EpiScore values for given mutation pairs, averaged over hACE2 binding sites. Cross-chain residue pairs in the upper right tend to be highly epistatic, similar to pairwise second-order interaction coefficients from Moulana et al. (Nature comm 2022).

365

366

367 **Episcore highlights the epistatic relationship between the recent adaptive mutations in VOCs and the**

368 **CAPs of the Wuhan reference.**

369 Seeking further to understand the role of epistasis within S protein variants, we explored the possibility

370 of epistatic relationships between the CAPs of the Wuhan variant and the new CAPs in VOCs. Thus, we

371 computed the EpiScore of these CAP positions in the closed RBD domains (i.e., chain B and C) with respect

372 to functional hACE2 binding interface sites of the open RBD domain chain (chain A) (Figure 5B) and

373 obtained EpiScore distributions.

374

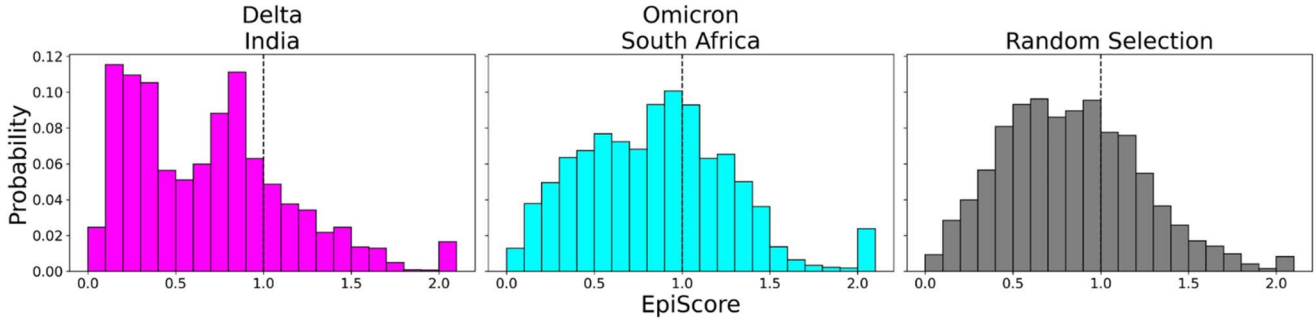

375

376 **Figure 6**. EpiScores with i = low EP Delta mutation sites (magenta), low EP Omicron mutation sites (Cyan),

377 and a random selection of sites (gray), j = low EP sites in the Wuhan variant, and k = the binding interface

378 of the open chain. EpiScores using sites of either variant (Delta: M = 0.70, SD = 0.50, Omicron M = 0.86,

379 SD = 0.46) are significantly different (p<.001) from a set of EpiScores using random sites (M = 0.84, SD =

380 0.41), but the distribution for Delta variants differs much more from the other two. EpiScores for other

381 variants can be found in Supplementary Figure S2.

382

383 To contrast these variants, Omicron (Figure 6, cyan) shows a high proportion of additive mutations

384 compared to the Delta variant (Figure 6, magenta), with a peak centered on 1. The comparatively more

385 pathogenic Delta variant exhibited many non-additive mutations with EpiScores below one. This again

386 suggests that the cross-communication between the open and closed chain of the S protein is important
387 for regulating the function. Four out of seven low EP Delta mutation sites used in this analysis often
388 resulted in EpiScores below 1. Each of those is found in the N-terminal domain (NTD) on or near the N3
389 loop and is implicated in antibody escape in recent studies (Chi et al. 2020; Weisblum et al. 2020; Harvey,
390 Carabelli, Jackson, Gupta, Thomson, Harrison, Ludden, Reeve, Rambaut, COVID-19 Genomics UK (COG-
391 UK) Consortium, et al. 2021; Klinakis et al. 2021; Cantoni et al. 2022). The low EpiScores of NTD mutations
392 suggest that they dampen the control of Wuhan variant CAPs over the hACE2 binding sites in addition to
393 their effects on antibody binding. It is possible that what the Delta variant gained in transmission rate also
394 came with being more harmfully pathogenic due in part to negatively epistatic interactions. In contrast,
395 the mutations leading to the development of the Omicron strain were additive with respect to Wuhan
396 variant CAPs, possibly leading to a lower pathogenicity and higher effective immune escape, resulting in
397 an overall higher transmission rate. Another possible explanation for the higher transmission rate of
398 Omicron comes from a different normal mode analysis study, which found that despite reduced binding
399 affinity with hACE2, Omicron showed increased occupancy of the open state compared to the closed state,
400 which would increase chances of interaction with hACE2 (Natalia Teruel et al. 2021). It is worth noting
401 that other variants contain NTD mutations which result in low EpiScores, however the proportion of these
402 mutations within the set is considerably less than in Delta (Supplementary Figure S3).
403 One of the more notable features of generated EpiScore distributions is the presence of a tail of values
404 upward of 2.0, indicating highly epistatic behavior. Interestingly, these tails are largely due to three
405 different CAPs: 346R, 486F, and 498Q. Those residues are nearby one another within the protein structure
406 and have been reported to play a role in antibody binding, either being known antibody binding sites
407 (346R and 486F) or having received very high antibody accessibility scores (498Q) (Harvey, Carabelli,
408 Jackson, Gupta, Thomson, Harrison, Ludden, Reeve, Rambaut, COVID-19 Genomics UK (COG-UK)
409 Consortium, et al. 2021; Raghuvamsi et al. 2021). These observed high EpiScore values also support other

410 studies indicating the epistatic interactions between these CAPs and the mutations of the VOCs within the
411 S protein are crucial for maintaining binding affinity of hACE2 whilst evading immunity (Hong et al. 2022;
412 Moulana et al. 2022b; Starr, Greaney, Stewart, et al. 2022).
413 Inspection of EpiScores of Delta and Omicron potentially adaptive mutation sites with only CAP site 486F
414 (a binding site for both hACE2 and antibodies) (Huang et al. 2020; Ali et al. 2021; Harvey, Carabelli,
415 Jackson, Gupta, Thomson, Harrison, Ludden, Reeve, Rambaut, COVID-19 Genomics UK (COG-UK)
416 Consortium, et al. 2021; Raghuvamsi et al. 2021) shows highly epistatic interactions at other hACE2
417 binding sites (Figure 6). However, within a recent and rapidly spreading subvariant of Omicron, XBB 1.5,
418 we see a mutation of S to P, a rare double nucleotide mutation, at site 486 (preceeding Omicron variants
419 included mutation F486S from the original CAP). This new variant has unprecedented immune escape
420 capabilities, resisting neutralizing antibodies almost entirely (Qu et al. 2023). EpiScores of other XBB 1.5
421 specific mutation sites with 486P are almost entirely greater than 1, showing an even higher degree of
422 epistasis with the binding sites of RBD (Figure 7). These results present a threefold importance for the
423 S486P mutation: Not only does this residue alter antibody (i.e., immune escape) and hACE2 binding by
424 directly modifying a binding site, but it may also be responsible for modifying hACE2 binding via epistatic
425 cooperation with other co-occurring mutations.

426

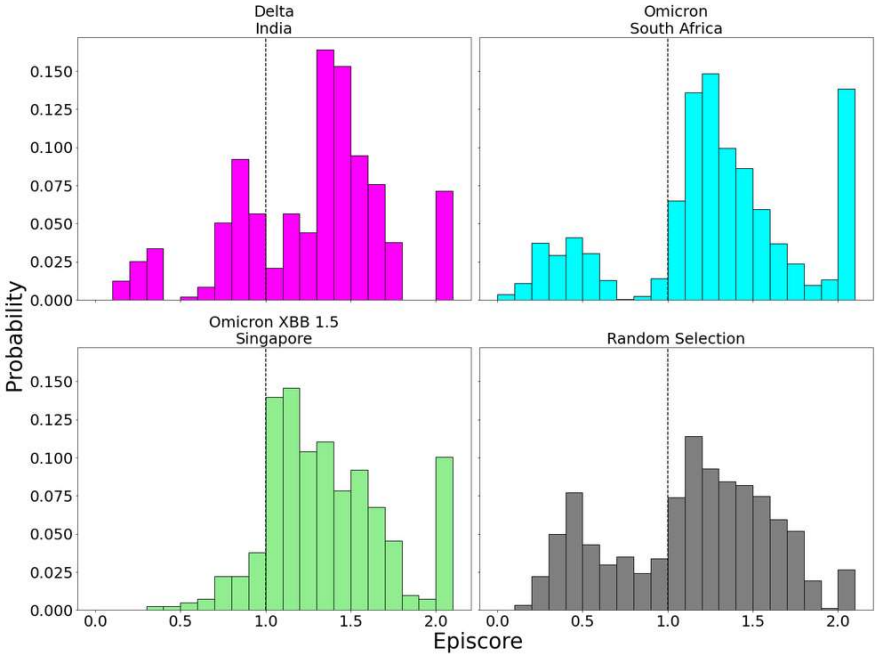

Figure 7. EpiScores with i = low EP Delta mutation sites (magenta), low EP Omicron mutation sites (Cyan), and a random selection of sites (gray), j = site 486, and k = the binding interface of the open chain. CAP and hACE2 and antibody binding site 486 displays epistasis with almost all XBB 1.5 variant sites at almost every hACE2 binding site (M = 1.40, SD = 0.46) and presents a significantly different profile from other variant sites (p <.01). EpiScores involving 486 for other variants can be found in Supplementary Figure S4.

Change in flexibility of RBD binding site correlates with experimental binding affinities for Omicron and Omicron XBB variants.

Experimental studies have tracked hACE2 binding for different variants since the virus first spread (Ali et al. 2021; Barton et al. 2021; Ozono et al. 2021; Wu et al. 2022). Within the Omicron variant, for example, characteristic mutations on the RBD are shown to increase the overall binding affinity of the virus to the ACE2 receptor, which is suspected to allow it to spread more easily (Kim et al. 2021). Furthermore, the new Omicron XBB and Omicron XBB 1.5 variants contain additional mutations in the RBD and antibody binding residues, which may further impact their dynamics and interactions with the host.

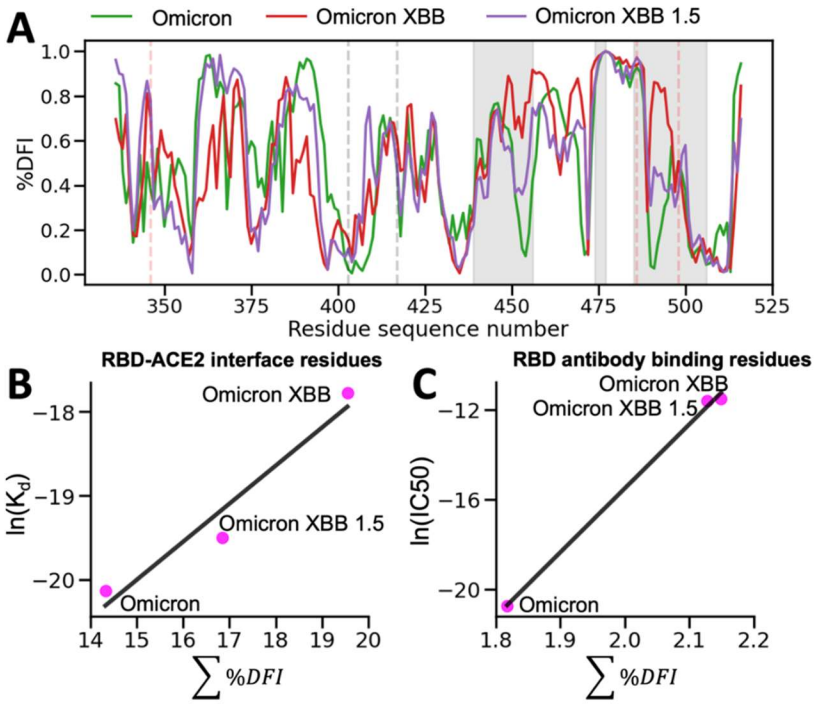

Figure 8. The %DFI calculations for variants Omicron, XBB, and XBB 1.5. (A) %DFI profile of the variants are plotted in the same panel. The grey shaded areas and dashed lines indicate the ACE2 binding regions, whereas the red dashed lines show the antibody binding residues. (B) The sum of %DFI values of RBD-ACE2 interface residues. The trend of total %DFI with the log of K_d values overlaps with the one seen with the experiments (R=0.97). (C) The RBD antibody binding residues are used to calculate the sum of %DFI. The ranking captured with the total %DFI agrees with the log of IC50 values from the experiments.

458

459 To gain deeper insights into the impact of dynamics on the binding affinity of hACE2 and antibodies with
460 the recent Omicron XBB variants, we conducted molecular dynamics (MD) simulations. By analyzing the
461 resulting trajectories, we investigated how these mutations influence the flexibility and rigidity of the RBD
462 and antibody binding residues, consequently affecting their binding affinity and potential for immune
463 evasion (Figure 8). To understand the overall flexibility changes, we measured the sum of DFI of the ACE2
464 binding residues, as well as the sum of DFI of the antibody binding residues, calculated from the MD
465 trajectories and compared then with experimental viral binding (disassociation constants) and immunity
466 evasion antibody IC50 values (Yue et al. 2023).
467 This investigation elucidated the impact of mutations in the RBD and antibody binding residues on the
468 binding affinity of the S protein and immune evasion by modulating their flexibility and rigidity (Figure
469 8A). The Omicron XBB variant exhibits heightened flexibility in hACE2 and antibody binding residues,
470 reducing infectivity and enhancing immune evasion. Conversely, the Omicron XBB 1.5 variant induces
471 distinct dynamics in these regions, rendering the RBD-ACE2 interface more rigid while increasing flexibility
472 in antibody binding residues. These effects indicate that Omicron XBB 1.5 retains its antibody escape
473 capabilities while regaining ACE2 binding affinity comparable to previous Omicron variants, in accordance
474 with experimental findings (Yue et al. 2023). These findings suggest that mutations in the RBD and
475 antibody binding residues can have complex effects on the dynamics of the protein and, ultimately, on
476 the virus's ability to infect and evade the host immune system through an alteration of binding site
477 dynamics. However, we do note that the effect of mutations will heavily depend on the genetic
478 background in which they are mutated. The effects of a mutation on a Delta variant protein may differ
479 entirely from the effects of a mutation on an Omicron variant protein (Supplementary figure S5).

480

481 **Conclusion:**

482 We analyzed the evolutionary trajectory of the CoV-2 S protein in humans to understand the dynamic
483 and epistatic interactions of the mutations defining specific VOCs. We first obtain the phylogenetic tree
484 of the COV-2 S protein and identify the sites of certain recent mutations known as candidate adaptive
485 polymorphisms (CAPs). CAPs are considered adaptive because mutations rarely tolerated in closely
486 related sequences have suddenly become fixed, implying a degree of functional importance or evolution
487 (Liu et al. 2016). In addition, our earlier work has shown that CAPS can also be compensatory; multiple
488 CAPs may dynamically compensate for one another, changing the dynamic landscape and allowing for
489 different mutations (Ose, Campitelli, et al. 2022). We then explored the mechanistic insights and
490 epistatic relationship between the observed mutations in different VOCs and CAP sites, and, particularly,
491 the relationship between CAP sites and the functionally critical RBD using our dynamic coupling analysis
492 (Kumar, A., Glembo, T.J., Ozkan, S.B. 2015b).

493 We find a mechanistic pattern in the S protein evolution that is common amongst previously studied
494 systems, where allosteric sites exert control over the dynamics of the binding sites, and mutations of
495 these allosteric sites modulate function. Coupling our analysis with evolutionary theory showed that
496 many of these allosteric sites regulating function of the S protein may have been subjected to adaptive
497 evolution as observed in mutations in VOCs. Our dynamics analysis also provides a mechanistic insight
498 where the Omicron defining sites have greater control over the binding sites than the Delta variant, and
499 are dynamically additive with the functional advantage of CAPs, thus, the greatest infectivity may not be
500 a coincidence.

501 Specifically, we find that the interactions between CAP sites and VOC-defining mutations show
502 fingerprints of non-additive dynamics within the Delta variant. In contrast, mutations leading to the
503 Omicron variant are largely additive, driving critical dynamical behavior closer to the patterns observed
504 within the wild-type. These interactions may also drive observed behavior similar between the reference
505 and Omicron strains yet differ in the delta strain, such as the severity of infection as evidenced by

506 hospitalization rates (Houhamdi et al. 2022; Menni et al. 2022). It has also been shown that the Omicron
507 variant has a lower binding affinity with hACE2 than previous variants (Wu et al. 2022), which may
508 contribute to its low pathogenecity.

509 Long-ranged interactions between different sites within a given protein is critically important for protein
510 function (Peters and Lively 1999; Bershtein et al. 2006; Collins et al. 2006; Ekeberg et al. 2013; Levy et al.
511 2017; Harrigan et al. 2018; Otten et al. 2018; Rojas Echenique et al. 2019; Shimagaki and Weigt 2019; de
512 la Paz et al. 2020; Rizzato et al. 2020; Yang et al. 2020; Bisardi et al. 2022) and for the CoV-2 S protein in
513 particular (Zeng et al. 2020; Castiglione et al. 2021; Dong et al. 2021; Garvin et al. 2021; Nielsen et al.
514 2022; Ramarao-Milne et al. 2022; Rochman et al. 2022; Rodriguez-Rivas et al. 2022). By showing dynamic
515 differences between the interactions of CAPs, which have likely played a major role in allowing the virus
516 to infect human hosts, the binding site, and the characteristic mutations of dominant Delta and Omicron
517 strains, we see a "fine-tuning" of protein behavior. As variants continue to evolve, Omicron sub-variants
518 are of growing concern due in large part to further increased immune evasion (Callaway 2022; Wang, Guo,
519 et al. 2022; Wang, Iketani, et al. 2022), and we observe that the new mutations observed in antibody
520 binding sites yield more epistatic interaction with the CAPs. In addition to supporting previous dynamic
521 research on the S protein, this analysis provides the insight that CAP sites are of continued importance to
522 protein function and should be given special attention when considering the impact of future mutations.
523

524 **Methods**

525

526 **Dynamic Flexibility and Dynamic Coupling**

527 The Dynamic Flexibility Index utilizes a Perturbation Response Scanning technique that combines the Elas-
528 tic Network Model (ENM) and Linear Response Theory (LRT) (Gerek and Ozkan 2011; Nevin Gerek, Z.,
529 Kumar, S., Banu Ozkan, S. 2013). In ENM, the protein is considered as a network of beads at Cα positions

interacting with each other via a harmonic spring potential. Using LRT, Δ**R** is calculated as the fluctuation response vector of residue *j* due to unit force's **F** perturbation on residue *i,* averaged over multiple unit force directions to simulate an isotropic perturbation.

$$[\Delta\mathbf{R}]_{3N\times1} = [\mathbf{H}]^{-1}_{3N\times3N}[\mathbf{F}]_{3N\times1} \tag{1}$$

H is the Hessian, a 3N × 3N matrix that can be constructed from 3-D atomic coordinate information and is composed of the second derivatives of the harmonic potential with respect to the components of the position's vectors of length 3N. The hessian inverse in this equation may be replaced with the covariance matrix **G** obtained from MD simulations as follows.

$$[\Delta\mathbf{R}]_{3N\times1} = [\mathbf{G}]_{3N\times3N}[\mathbf{F}]_{3N\times1} \tag{2}$$

MD simulations were used to obtain the DFI profiles of Omicron, Omicron XBB, and Omicron XBB 1.5. In order to obtain DFI, each position in the structure was perturbed sequentially to generate a Perturbation Response Matrix ***A***

$$\mathbf{A}_{N\times N} = \begin{bmatrix} |\Delta R^1|_1 & \cdots & |\Delta R^N|_1 \\ \vdots & \ddots & \vdots \\ |\Delta R^1|_N & \cdots & |\Delta R^N|_N \end{bmatrix} \tag{3}$$

where $|\Delta R^j|_i = \sqrt{\langle(\Delta R)^2\rangle}$ is the magnitude of fluctuation response at position *i* due to perturbations at position *j. T*he DFI value of position *i* is then treated as the displacement response of position *i* relative to

551 the net displacement response of the entire protein, which is calculated by sequentially perturbing each

552 position in the structure.

553

555 $$\mathrm{DFI_i} = \frac{\sum_{j=1}^{N} \left|\Delta R^j\right|_i}{\sum_{i=1}^{N} \sum_{j=1}^{N} \left|\Delta R^j\right|_i}$$

554 (4)

556 It is also often useful to quantify position flexibility relative to the flexibility ranges unique to individual

557 structures. To that end, DFI can be presented as a percentile rank, %DFI. All %DFI calculations present in

558 this work used the DFI value of every residue of the full spike structure for ranking. The DFI parameter can

559 be considered a measure of a given amino acid position's ability to explore its local conformational space.

560

561 **Dynamic Coupling Index**

562 Similar to DFI, the dynamic coupling index (DCI) (Larrimore et al. 2017; Kumar, A., Glembo, T.J., Ozkan,

563 S.B. 2015b) also utilizes Perturbation Response Scanning with the Elastic Network Model and Linear

564 Response Theory. DCI captures the strength of displacement response of a given position *i* upon

565 perturbation to a single functionally important position (or subset of positions) *j*, relative to the average

566 fluctuation response of position *i* when all of the positions within a structure are perturbed.

567

570 $$\mathrm{DCI_{ji}} = \frac{\sum_{j}^{N_{functional}} \left|\Delta R^j\right|_i / N_{functional}}{\sum_{j=1}^{N} \left|\Delta R^j\right|_i / N}$$

568 (5)

569 When only positional pairs are concerned, this expression reduces to:

571

573 $$\mathrm{DCI_{ji}} = \frac{\left|\Delta \mathrm{R^j}\right|_\mathrm{i}}{\sum_{\mathrm{j=1}}^{\mathrm{N}} \left|\Delta \mathrm{R^j}\right|_\mathrm{i} / \mathrm{N}}$$

572 (6)

574 As such, this parameter represents a measure of the dynamic coupling between *i* and *j* upon a
575 perturbation to *j.* As with DFI, DCI_{ji} can also be presented as a percentile-ranked $\%DCI_{ji}$.

576 One of the most important aspects of DCI is that the entire network of interactions is explicitly included
577 in subsequent calculations without the need for dimensionality reduction techniques. If one considers
578 interactions such as communication directionality or dynamic coupling regulation between position pairs
579 as inherent properties of an anisotropic interaction network, it is critical to include the interactions of the
580 entire network to accurately model the effect one residue can have on another.

581 Here, we present two further extensions of DCI which allow us to uniquely model coupling directionality
582 and epistatic effects: DCI_{asym} and EpiScore, respectively. Interestingly, we can capture asymmetry between
583 different residues within a protein through DCI, as a coupling in and of itself is asymmetric within an ani-
584 sotropic network. That is, each amino acid has a set of positions to which it is highly coupled, and this
585 anisotropy in connections gives rise to unique differences in coupling between a given *i j* pair of amino
586 acids which do not have direct interactions (Figure 2A). DCI_{asym}, then, is simply DCI_{ij} (the normalized dis-
587 placement response of position *j* upon a perturbation to position *i*) − DCI_{ji} (Equation (7)). Using DCI_{asym} we
588 can determine a cause-effect relationship between the *i j* pair in terms of force/signal propagation be-
589 tween these two positions.

590

592 $$\mathrm{DCI_{asym}} = \mathrm{DCI_{ij}} - \mathrm{DCI_{ji}}$$

591 (7)

594 $$\%\mathrm{DCI}_{\mathrm{asym}} = \%\mathrm{DCI}_{\mathrm{ij}} - \%\mathrm{DCI}_{\mathrm{ji}}$$

593 (8)

595 where a positive $\mathrm{DCI}_{\mathrm{asym}}$ value indicates communication from position *i* to position *j.*

596 EpiScore can identify or describe potential non-additivity in substitution behavior between residue pairs.
597 This metric can capture the differences in a normalized perturbation response to a position *k* when a force
598 is applied at two residues *i* and *j* simultaneously versus the average additive perturbation response when
599 each residue *i*, *j*, is perturbed individually (Figure 5A, Equation 9).

601 $$\mathrm{EpiScore} = \frac{\%\mathrm{DCI}_{[\mathrm{ij}]\mathrm{k}}}{\frac{1}{2}\left(\%\mathrm{DCI}_{\mathrm{ik}} + \%\mathrm{DCI}_{\mathrm{jk}}\right)}$$

600 (9)

602 EpiScore values < 1 (> 1) indicate that the additive perturbations of positions *i* and *j* generates a greater
603 (lesser) response at position *k* than the effect of a simultaneous perturbation. This means that, when
604 treated with a simultaneous perturbation at both sites i and j, the displacement response of k is lower
605 (higher) than the average effect of individual perturbations to *i* and *j*, one at a time. As EpiScore is a linear
606 scale, the further the value from 1, the greater the effect described above.

607 **Molecular Dynamics (MD)**

608 The production simulations for the Omicron variants, including Omicron, Omicron XBB, and Omicron XBB
609 1.5, were performed with the AMBER software package. These variants, each characterized by specific
610 mutations, were modeled based on the template PDB structure 6M0J. The initial protein configurations
611 in the simulations were parameterized using the ff14SB force field (Maier et al. 2015). In order to create
612 an appropriate solvation environment for the proteins, a solvation box was defined around them, main-

613 taining a minimum separation distance of 16Å from the protein to the box boundaries. This was accom-
614 plished by employing the explicit TIP3P water model (Sun 1995), with the addition of sodium and chloride
615 ions to maintain overall charge neutrality.
616 The simulation procedure involves an initial energy minimization step, aimed at mitigating steric clashes
617 and optimizing the system's energy. A steepest descent algorithm was applied, encompassing 11,000
618 steps. Subsequently, the system underwent a gradual temperature increase (heat up),up to 300K, and
619 was subjected to production simulations under a constant number of particles, pressure, and temperature
620 ensemble (NPT).
621 During these production simulations, temperature was maintained at 300K, with pressure regulation set
622 at 1 bar. Temperature regulation was achieved through the utilization of the Langevin thermostat (Hü-
623 nenberger 2005) and Berendsen barostat (Berendsen et al. 1984), featuring a collision frequency of 1.0
624 picoseconds^{-1}. Hydrogen atom bond lengths were constrained using the SHAKE algorithm (Pearlman et al.
625 1995). The production trajectories were simulated for 1µs each.
626 To ensure the reliability of the simulations and assess their convergence, a convergence criterion was
627 employed. The achieved convergence was determined by monitoring the root mean square deviation
628 (RMSD) between the highest sampled conformation in consecutive time windows (Sawle and Ghosh
629 2016). Specifically, convergence was defined as the point at which the RMSD between the highest sam-
630 pled conformation in the last 300 nanoseconds (ns) window and the 300ns window immediately preced-
631 ing it dropped below 1 angstrom (Å). Window sizes varying from 100ns to 500ns were employed to eval-
632 uate convergence, ensuring the robustness and stability of the obtained results.

633 To calculate DFI, covariance matrix data were computed over different time windows as discussed
634 above. By default, utilizing the Hessian implies a restriction to a harmonic potential, assuming that the
635 data are sampled from a Gaussian distribution. Ergodicity in both simulation time and initial structures
636 sampled in each time interval ensures two key conditions: (i) Consistency of potential energy across

637 conformations sampled from the same distribution. (ii) The sampling of different initial conformations
638 while computing covariance matrices at various time windows eliminates global motions and accurately
639 captures equilibrium coordinates. Consequently, the final average DFI profiles are independent of time
640 window size, resulting in consistent results across different time window sizes (e.g., 50 ns vs. 75 ns) and
641 enabling the acquisition of statistically significant DFI values.

642 **Data and Resource Availability**

643 The code to perform DFI and DCI analysis is available at https://github.com/SBOZKAN/DFI-DCI.
644 Molecular Dynamics data are available upon request. The mutation sites and EP values are contained in
645 the supporting information files as "Supplementary_mutation_info.csv". The alignment used to
646 generate EP values is also contained within the supporting information files as "EP_alignment.fas".
647 Protein Databank ID number 6VXX (Walls et al. 2020) was used for closed conformation DCI calculations.
648 6VSB (Wrapp et al. 2020) was used for DFI calculations, EpiScore calculations, and open conformation
649 DCI calculations. 6M0J (Lan et al. 2020) was used in molecular dynamics simulations of the RBD.

650 **Acknowledgements**

651 Funding was provided to N.J.O., P.C., T.M., and I.C.K. by the Gordon and Betty Moore Foundation (award
652 number AWD00034439) and to S.B.O. by the National Science Foundation (award numbers: 1715591
653 and 1901709) and the National Institutes of Health R01GM147635-01. S.K. acknowledges the National
654 Science Foundation (GCR 1934848) and the National Institutes of Health (GM139540) grants.

655 **References:**

656 Abduljalil JM, Elghareib AM, Samir A, Ezat AA, Elfiky AA. 2023. How helpful were molecular dynamics
657 simulations in shaping our understanding of SARS-CoV-2 spike protein dynamics? *Int. J. Biol.*
658 *Macromol.* 242:125153.

659 Ali F, Kasry A, Amin M. 2021. The new SARS-CoV-2 strain shows a stronger binding affinity to ACE2 due
660 to N501Y mutant. *Med. Drug Discov.* 10:100086.

661 Amicone M, Borges V, Alves MJ, Isidro J, Zé-Zé L, Duarte S, Vieira L, Guiomar R, Gomes JP, Gordo I. 2022.
662 Mutation rate of SARS-CoV-2 and emergence of mutators during experimental evolution. *Evol.*
663 *Med. Public Health* 10:142–155.

664 Barton MI, MacGowan SA, Kutuzov MA, Dushek O, Barton GJ, van der Merwe PA. 2021. Effects of
665 common mutations in the SARS-CoV-2 Spike RBD and its ligand, the human ACE2 receptor on
666 binding affinity and kinetics. *eLife* 10:e70658.

667 Berendsen HJC, Postma JPM, van Gunsteren WF, DiNola A, Haak JR. 1984. Molecular dynamics with
668 coupling to an external bath. *J. Chem. Phys.* 81:3684–3690.

669 Berman, H.M., Westbrook, J., Feng, Z., Gilliland, G., Bhat, T.N., Weissig, H., Shindyalov, I.N., Bourne, P.E.
670 2000. The Protein Data Bank. *Nucleic Acids Res* 28:235–242.

671 Bershtein S, Segal M, Bekerman R, Tokuriki N, Tawfik DS. 2006. Robustness–epistasis link shapes the
672 fitness landscape of a randomly drifting protein. *Nature* 444:929–932.

673 Bhabha G, Ekiert DC, Jennewein M, Zmasek CM, Tuttle LM, Kroon G, Dyson HJ, Godzik A, Wilson IA,
674 Wright PE. 2013. Divergent evolution of protein conformational dynamics in dihydrofolate
675 reductase. *Nat. Struct. Mol. Biol.* 20:1243–1249.

676 Bisardi M, Rodriguez-Rivas J, Zamponi F, Weigt M. 2022. Modeling Sequence-Space Exploration and
677 Emergence of Epistatic Signals in Protein Evolution.Ozkan B, editor. *Mol. Biol. Evol.* 39:msab321.

678 Boni MF, Lemey P, Jiang X, Lam TT-Y, Perry BW, Castoe TA, Rambaut A, Robertson DL. 2020. Evolutionary
679 origins of the SARS-CoV-2 sarbecovirus lineage responsible for the COVID-19 pandemic. *Nat.*
680 *Microbiol.* 5:1408–1417.

681 Brister JR, Ako-adjei D, Bao Y, Blinkova O. 2015. NCBI Viral Genomes Resource. *Nucleic Acids Res.*
682 43:D571–D577.

683 Butler BM, Kazan IC, Kumar A, Ozkan SB. 2018. Coevolving residues inform protein dynamics profiles and
684 disease susceptibility of nSNVs.Jernigan RL, editor. *PLOS Comput. Biol.* 14:e1006626.

685 Cagliani R, Forni D, Clerici M, Sironi M. 2020. Computational Inference of Selection Underlying the
686 Evolution of the Novel Coronavirus, Severe Acute Respiratory Syndrome Coronavirus 2.Gallagher
687 T, editor. *J. Virol.* 94:e00411-20.

688 Callaway E. 2022. COVID 'variant soup' is making winter surges hard to predict. *Nature* 611:213–214.

689 Campbell, E., Kaltenbach, M., Correy, G., Carr, P., Porebski, B.T., Livingstone, E., Jurnou, L., Hyvönen, M.,
690 Buckle, A.M., Weik, M., et al. 2016. The role of protein dynamics in the evolution of new enzyme
691 function. *Nat Chem Biol*.

692 Campitelli P, Lu J, Ozkan SB. 2022. Dynamic allostery highlights the evolutionary differences between the
693 CoV-1 and CoV-2 main proteases. *Biophys. J.* 121:1483–1492.

694 Campitelli P, Modi T, Kumar S, Ozkan SB. The Role of Conformational Dynamics and Allostery in
695 Modulating Protein Evolution. *Annu. Rev. Biophys.* 49:267–288.

696 Campitelli P, Modi T, Kumar S, Ozkan SB. 2020a. The Role of Conformational Dynamics and Allostery in
697 Modulating Protein Evolution. *Annu. Rev. Biophys.* 49:267–288.

698 Campitelli P, Ozkan SB. 2020. Allostery and Epistasis: Emergent Properties of Anisotropic Networks.
699 *Entropy* 22:667.

700 Campitelli P, Swint-Kruse L, Ozkan SB. 2020b. Substitutions at Nonconserved Rheostat Positions
701 Modulate Function by Rewiring Long-Range, Dynamic Interactions.Wilke C, editor. *Mol. Biol.*
702 *Evol.* 38:201–214.

703 Cantoni D, Murray MJ, Kalemera MD, Dicken SJ, Stejskal L, Brown G, Lytras S, Coey JD, McKenna J,
704 Bridgett S, et al. 2022. Evolutionary remodelling of N-terminal domain loops fine-tunes SARS-
705 CoV -2 spike. *EMBO Rep.* [Internet] 23. Available from:
706 https://onlinelibrary.wiley.com/doi/10.15252/embr.202154322

707 Carabelli AM, Peacock TP, Thorne LG, Harvey WT, Hughes J, COVID-19 Genomics UK Consortium, De
708 Silva TI, Peacock SJ, Barclay WS, De Silva TI, et al. 2023. SARS-CoV-2 variant biology: immune
709 escape, transmission and fitness. *Nat. Rev. Microbiol.* [Internet]. Available from:
710 https://www.nature.com/articles/s41579-022-00841-7

711 Castiglione GM, Zhou L, Xu Z, Neiman Z, Hung C-F, Duh EJ. 2021. Evolutionary pathways to SARS-CoV-2
712 resistance are opened and closed by epistasis acting on ACE2.Hejnol A, editor. *PLOS Biol.*
713 19:e3001510.

714 Chan C-M, Woo PCY, Lau SKP, Tse H, Chen H-L, Li F, Zheng B-J, Chen L, Huang J-D, Yuen K-Y. 2008. Spike
715 Protein, S, of Human Coronavirus HKU1: Role in Viral Life Cycle and Application in Antibody
716 Detection. *Exp. Biol. Med.* 233:1527–1536.

717 Changeux J-P, Edelstein SJ. 2005. Allosteric Mechanisms of Signal Transduction. *Science* 308:1424–1428.

718 Chi X, Yan R, Zhang Jun, Zhang G, Zhang Y, Hao M, Zhang Z, Fan P, Dong Y, Yang Y, et al. 2020. A
719 neutralizing human antibody binds to the N-terminal domain of the Spike protein of SARS-CoV-
720 2. *Science* 369:650–655.

721 Collins SR, Schuldiner M, Krogan NJ, Weissman JS. 2006. A strategy for extracting and analyzing large-
722 scale quantitative epistatic interaction data. *Genome Biol.* 7:R63.

723 Damas J, Hughes GM, Keough KC, Painter CA, Persky NS, Corbo M, Hiller M, Koepfli K-P, Pfenning AR,
724 Zhao H, et al. 2020. Broad host range of SARS-CoV-2 predicted by comparative and structural
725 analysis of ACE2 in vertebrates. *Proc. Natl. Acad. Sci.* 117:22311–22322.

726 Deng X, Garcia-Knight MA, Khalid MM, Servellita V, Wang C, Morris MK, Sotomayor-González A, Glasner
727 DR, Reyes KR, Gliwa AS, et al. 2021. Transmission, infectivity, and antibody neutralization of an
728 emerging SARS-CoV-2 variant in California carrying a L452R spike protein mutation. Infectious
729 Diseases (except HIV/AIDS) Available from:
730 http://medrxiv.org/lookup/doi/10.1101/2021.03.07.21252647

731 Díaz-Salinas MA, Li Q, Ejemel M, Yurkovetskiy L, Luban J, Shen K, Wang Y, Munro JB. 2022.
732 Conformational dynamics and allosteric modulation of the SARS-CoV-2 spike. *eLife* 11:e75433.

733 Dicken SJ, Murray MJ, Thorne LG, Reuschl A-K, Forrest C, Ganeshalingham M, Muir L, Kalemera MD,
734 Palor M, McCoy LE, et al. 2021. Characterisation of B.1.1.7 and Pangolin coronavirus spike
735 provides insights on the evolutionary trajectory of SARS-CoV-2. Microbiology Available from:
736 http://biorxiv.org/lookup/doi/10.1101/2021.03.22.436468

737 Dong A, Zhao J, Griffin C, Wu R. 2021. The Genomic Physics of COVID-19 Pathogenesis and Spread. *Cells*
738 11:80.

739 Doshi U, Holliday MJ, Eisenmesser EZ, Hamelberg D. 2016. Dynamical network of residue–residue
740 contacts reveals coupled allosteric effects in recognition, catalysis, and mutation. *Proc. Natl.*
741 *Acad. Sci.* 113:4735–4740.

742 Dror RO, Dirks RM, Grossman JP, Xu H, Shaw DE. 2012. Biomolecular Simulation: A Computational
743 Microscope for Molecular Biology. *Annu. Rev. Biophys.* 41:429–452.

744 Ekeberg M, Lövkvist C, Lan Y, Weigt M, Aurell E. 2013. Improved contact prediction in proteins: Using
745 pseudolikelihoods to infer Potts models. *Phys. Rev. E* 87:012707.

746 Fraser BJ, Beldar S, Seitova A, Hutchinson A, Mannar D, Li Y, Kwon D, Tan R, Wilson RP, Leopold K, et al.
747 2022. Structure and activity of human TMPRSS2 protease implicated in SARS-CoV-2 activation.
748 *Nat. Chem. Biol.* 18:963–971.

749 Frost SDW, Magalis BR, Kosakovsky Pond SL. 2018. Neutral Theory and Rapidly Evolving Viral
750 Pathogens.Kumar S, editor. *Mol. Biol. Evol.* 35:1348–1354.

751 Garvin MR, Prates ET, Romero J, Cliff A, Machado Gazolla JGF, Pickholz M, Pavicic M, Jacobson D. 2021.
752 Rapid expansion of SARS-CoV-2 variants of concern is a result of adaptive epistasis. Evolutionary
753 Biology Available from: http://biorxiv.org/lookup/doi/10.1101/2021.08.03.454981

754 Gerek ZN, Ozkan SB. 2011. Change in Allosteric Network Affects Binding Affinities of PDZ Domains:
755 Analysis through Perturbation Response Scanning.Nussinov R, editor. *PLoS Comput. Biol.*
756 7:e1002154.

757 Gobeil SM-C, Janowska K, McDowell S, Mansouri K, Parks R, Manne K, Stalls V, Kopp MF, Henderson R,
758 Edwards RJ, et al. 2021. D614G Mutation Alters SARS-CoV-2 Spike Conformation and Enhances
759 Protease Cleavage at the S1/S2 Junction. *Cell Rep.* 34:108630.

760 Gobeil SM-C, Janowska K, McDowell S, Mansouri K, Parks R, Stalls V, Kopp MF, Manne K, Li D, Wiehe K,
761 et al. 2021. Effect of natural mutations of SARS-CoV-2 on spike structure, conformation, and
762 antigenicity. *Science* 373:eabi6226.

763 Gur M, Taka E, Yilmaz SZ, Kilinc C, Aktas U, Golcuk M. 2020. Conformational transition of SARS-CoV-2
764 spike glycoprotein between its closed and open states. *J. Chem. Phys.* 153:075101.

765 Harrigan P, Madhani HD, El-Samad H. 2018. Real-Time Genetic Compensation Defines the Dynamic
766 Demands of Feedback Control. *Cell* 175:877-886.e10.

767 Harvey WT, Carabelli AM, Jackson B, Gupta RK, Thomson EC, Harrison EM, Ludden C, Reeve R, Rambaut
768 A, Consortium C-19 GU (COG-U, et al. 2021. SARS-CoV-2 variants, spike mutations and immune
769 escape. *Nat. Rev. Microbiol.* 19:409–424.

770 Harvey WT, Carabelli AM, Jackson B, Gupta RK, Thomson EC, Harrison EM, Ludden C, Reeve R, Rambaut
771 A, COVID-19 Genomics UK (COG-UK) Consortium, et al. 2021. SARS-CoV-2 variants, spike
772 mutations and immune escape. *Nat. Rev. Microbiol.* 19:409–424.

773 Henderson R, Edwards RJ, Mansouri K, Janowska K, Stalls V, Gobeil SMC, Kopp M, Li D, Parks R, Hsu AL,
774 et al. 2020. Controlling the SARS-CoV-2 spike glycoprotein conformation. *Nat. Struct. Mol. Biol.*
775 27:925–933.

776 Hoffmann M, Kleine-Weber H, Schroeder S, Krüger N, Herrler T, Erichsen S, Schiergens TS, Herrler G, Wu
777 N-H, Nitsche A, et al. 2020a. SARS-CoV-2 Cell Entry Depends on ACE2 and TMPRSS2 and Is
778 Blocked by a Clinically Proven Protease Inhibitor. *Cell* 181:271-280.e8.

779 Hoffmann M, Kleine-Weber H, Schroeder S, Krüger N, Herrler T, Erichsen S, Schiergens TS, Herrler G, Wu
780 N-H, Nitsche A, et al. 2020b. SARS-CoV-2 Cell Entry Depends on ACE2 and TMPRSS2 and Is
781 Blocked by a Clinically Proven Protease Inhibitor. *Cell* 181:271-280.e8.

782 Hong Q, Han W, Li J, Xu S, Wang Yifan, Xu C, Li Z, Wang Yanxing, Zhang C, Huang Z, et al. 2022. Molecular
783 basis of receptor binding and antibody neutralization of Omicron. *Nature* 604:546–552.

784 Houhamdi L, Gautret P, Hoang VT, Fournier P, Colson P, Raoult D. 2022. Characteristics of the first 1119
785 SARS-CoV-2 Omicron variant cases, in Marseille, France, November−December 2021. *J. Med.*
786 *Virol.* 94:2290–2295.

787 Huang Y, Yang C, Xu X, Xu W, Liu S. 2020. Structural and functional properties of SARS-CoV-2 spike
788 protein: potential antivirus drug development for COVID-19. *Acta Pharmacol. Sin.* 41:1141–
789 1149.

790 Hünenberger PH. 2005. Thermostat Algorithms for Molecular Dynamics Simulations. In: Dr. Holm C, Prof.
791 Dr. Kremer K, editors. Advanced Computer Simulation. Vol. 173. Berlin, Heidelberg: Springer
792 Berlin Heidelberg. p. 105–149. Available from: http://link.springer.com/10.1007/b99427

793 Jackson CB, Farzan M, Chen B, Choe H. 2022. Mechanisms of SARS-CoV-2 entry into cells. *Nat. Rev. Mol.*
794 *Cell Biol.* 23:3–20.

795 Kazan IC, Mills JH, Ozkan SB. 2023. Allosteric regulatory control in dihydrofolate reductase is revealed by
796 dynamic asymmetry. *Protein Sci.* 32:e4700.

797 Kazan IC, Sharma P, Rahman MI, Bobkov A, Fromme R, Ghirlanda G, Ozkan SB. 2022. Design of novel
798 cyanovirin-N variants by modulation of binding dynamics through distal mutations. *eLife*
799 11:e67474.

800 Kemp SA, Collier DA, Datir RP, Ferreira IATM, Gayed S, Jahun A, Hosmillo M, Rees-Spear C, Mlcochova P,
801 Lumb IU, et al. 2021. SARS-CoV-2 evolution during treatment of chronic infection. *Nature*
802 592:277–282.

803 Keskin O, Bahar I, Jernigan RL, Beutler JA, Shoemaker RH, Sausville EA, Covell DG. 2000. Characterization
804 of anticancer agents by their growth inhibitory activity and relationships to mechanism of action
805 and structure. *Anticancer. Drug Des.* 15:79–98.

806 Khan A, Zia T, Suleman M, Khan T, Ali SS, Abbasi AA, Mohammad A, Wei D. 2021. Higher infectivity of the
807 SARS-CoV-2 new variants is associated with K417N/T, E484K, and N501Y mutants: An insight
808 from structural data. *J. Cell. Physiol.* 236:7045–7057.

809 Kim, H., Zou, T., Modi, C., Dörner, K., Grunkemeyer, T.J., Chen, L., Fromme, R., Matz, M. V., Ozkan, S.B.,
810 Wachter, R.M. 2015. A hinge migration mechanism unlocks the evolution of green-to-red
811 photoconversion in GFP-like proteins. *Structure* 23:34–43.

812 Kim Sinae, Nguyen TT, Taitt AS, Jhun H, Park H-Y, Kim S-H, Kim Y-G, Song EY, Lee Y, Yum H, et al. 2021.
813 SARS-CoV-2 Omicron Mutation Is Faster than the Chase: Multiple Mutations on Spike/ACE2
814 Interaction Residues. *Immune Netw.* 21:e38.

815 Kimura, Motoo. 1983. The neutral theory of molecular evolution. Cambridge University Press

816 Kirchdoerfer RN, Cottrell CA, Wang N, Pallesen J, Yassine HM, Turner HL, Corbett KS, Graham BS,
817 McLellan JS, Ward AB. 2016. Pre-fusion structure of a human coronavirus spike protein. *Nature*
818 531:118–121.

819 Kistler KE, Huddleston J, Bedford T. 2022. Rapid and parallel adaptive mutations in spike S1 drive clade
820 success in SARS-CoV-2. *Cell Host Microbe* 30:545-555.e4.

821 Klinakis A, Cournia Z, Rampias T. 2021. N-terminal domain mutations of the spike protein are structurally
822 implicated in epitope recognition in emerging SARS-CoV-2 strains. *Comput. Struct. Biotechnol. J.*
823 19:5556–5567.

824 Kolbaba-Kartchner B, Kazan IC, Mills JH, Ozkan SB. 2021. The Role of Rigid Residues in Modulating TEM-1
825 β-Lactamase Function and Thermostability. *Int. J. Mol. Sci.* 22:2895.

826 Kumar, A., Glembo, T.J., Ozkan, S.B. 2015b. The Role of Conformational Dynamics and Allostery in the
827 Disease Development of Human Ferritin. *Biophys J* 109:1273–1281.

828 Kumar S, Stecher G, Li M, Knyaz C, Tamura K. 2018. MEGA X: Molecular Evolutionary Genetics Analysis
829 across Computing Platforms.Battistuzzi FU, editor. *Mol. Biol. Evol.* 35:1547–1549.

830 Kumar S, Tao Q, Weaver S, Sanderford M, Caraballo-Ortiz MA, Sharma S, Pond SLK, Miura S. 2021. An
831 Evolutionary Portrait of the Progenitor SARS-CoV-2 and Its Dominant Offshoots in COVID-19
832 Pandemic.Yeager M, editor. *Mol. Biol. Evol.* 38:3046–3059.

833 Kuzmanic A, Bowman GR, Juarez-Jimenez J, Michel J, Gervasio FL. 2020. Investigating Cryptic Binding
834 Sites by Molecular Dynamics Simulations. *Acc. Chem. Res.* 53:654–661.

835 Labbadia J, Morimoto RI. 2015. The Biology of Proteostasis in Aging and Disease. *Annu. Rev. Biochem.*
836 84:435–464.

837 Laiton-Donato K, Franco-Muñoz C, Álvarez-Díaz DA, Ruiz-Moreno HA, Usme-Ciro JA, Prada DA, Reales-
838 González J, Corchuelo S, Herrera-Sepúlveda MT, Naizaque J, et al. 2021. Characterization of the
839 emerging B.1.621 variant of interest of SARS-CoV-2. *Infect. Genet. Evol.* 95:105038.

840 Lan J, Ge J, Yu J, Shan S, Zhou H, Fan S, Zhang Q, Shi X, Wang Q, Zhang L, et al. 2020. Structure of the
841 SARS-CoV-2 spike receptor-binding domain bound to the ACE2 receptor. *Nature* 581:215–220.

842 Larrimore KE, Kazan IC, Kannan L, Kendle RP, Jamal T, Barcus M, Bolia A, Brimijoin S, Zhan C-G, Ozkan SB,
843 et al. 2017. Plant-expressed cocaine hydrolase variants of butyrylcholinesterase exhibit altered
844 allosteric effects of cholinesterase activity and increased inhibitor sensitivity. *Sci. Rep.* 7:10419.

845 Levy RM, Haldane A, Flynn WF. 2017. Potts Hamiltonian models of protein co-variation, free energy
846 landscapes, and evolutionary fitness. *Curr. Opin. Struct. Biol.* 43:55–62.

847 Liu L, Tamura K, Sanderford M, Gray VE, Kumar S. 2016. A Molecular Evolutionary Reference for the
848 Human Variome. *Mol. Biol. Evol.* 33:245–254.

849 Liu Xueyan, Liu Xuan, Zhou J, Dong Y, Jiang Wen, Jiang Wenqing. 2022. Rampant C-to-U deamination
850 accounts for the intrinsically high mutation rate in SARS-CoV-2 spike gene. *RNA* 28:917–926.

851 Liu Y, Bahar I. 2012. Sequence Evolution Correlates with Structural Dynamics. *Mol. Biol. Evol.* 29:2253–
852 2263.

853 Ma B, Nussinov R. 2016. Conformational footprints. *Nat. Chem. Biol.* 12:890–891.

854 Maguid S, Fernandez-Alberti S, Echave J. 2008. Evolutionary conservation of protein vibrational
855 dynamics. *Gene* 422:7–13.

856 Maguid S, Fernández-Alberti S, Parisi G, Echave J. 2006. Evolutionary Conservation of Protein Backbone
857 Flexibility. *J. Mol. Evol.* 63:448–457.

858 Maher MC, Bartha I, Weaver S, Di Iulio J, Ferri E, Soriaga L, Lempp FA, Hie BL, Bryson B, Berger B, et al.
859 2022. Predicting the mutational drivers of future SARS-CoV-2 variants of concern. *Sci. Transl.*
860 *Med.* 14:eabk3445.

861 Maier JA, Martinez C, Kasavajhala K, Wickstrom L, Hauser KE, Simmerling C. 2015. ff14SB: Improving the
862 Accuracy of Protein Side Chain and Backbone Parameters from ff99SB. *J. Chem. Theory Comput.*
863 11:3696–3713.

864 Majumder S, Chaudhuri D, Datta J, Giri K. 2021. Exploring the intrinsic dynamics of SARS-CoV-2, SARS-
865 CoV and MERS-CoV spike glycoprotein through normal mode analysis using anisotropic network
866 model. *J. Mol. Graph. Model.* 102:107778.

867 Markov PV, Ghafari M, Beer M, Lythgoe K, Simmonds P, Stilianakis NI, Katzourakis A. 2023. The evolution
868 of SARS-CoV-2. *Nat. Rev. Microbiol.* 21:361–379.

869 Menni C, Valdes AM, Polidori L, Antonelli M, Penamakuri S, Nogal A, Louca P, May A, Figueiredo JC, Hu C,
870 et al. 2022. Symptom prevalence, duration, and risk of hospital admission in individuals infected

871 with SARS-CoV-2 during periods of omicron and delta variant dominance: a prospective
872 observational study from the ZOE COVID Study. *The Lancet* 399:1618–1624.

873 Mikulska-Ruminska K, Shrivastava I, Krieger J, Zhang S, Li H, Bayır H, Wenzel SE, VanDemark AP, Kagan
874 VE, Bahar I. 2019. Characterization of Differential Dynamics, Specificity, and Allostery of
875 Lipoxygenase Family Members. *J. Chem. Inf. Model.* 59:2496–2508.

876 Millet JK, Whittaker GR. 2014. Host cell entry of Middle East respiratory syndrome coronavirus after
877 two-step, furin-mediated activation of the spike protein. *Proc. Natl. Acad. Sci.* 111:15214–
878 15219.

879 Millet JK, Whittaker GR. 2015. Host cell proteases: Critical determinants of coronavirus tropism and
880 pathogenesis. *Virus Res.* 202:120–134.

881 Mishra SK, Jernigan RL. 2018. Protein dynamic communities from elastic network models align closely to
882 the communities defined by molecular dynamics.Zhang Y, editor. *PLOS ONE* 13:e0199225.

883 Modi T, Campitelli P, Kazan IC, Ozkan SB. 2021. Protein folding stability and binding interactions through
884 the lens of evolution: a dynamical perspective. *Curr. Opin. Struct. Biol.* 66:207–215.

885 Modi T, Ozkan S. 2018. Mutations Utilize Dynamic Allostery to Confer Resistance in TEM-1 β-lactamase.
886 *Int. J. Mol. Sci.* 19:3808.

887 Modi T, Risso VA, Martinez-Rodriguez S, Gavira JA, Mebrat MD, Van Horn WD, Sanchez-Ruiz JM, Banu
888 Ozkan S. 2021. Hinge-shift mechanism as a protein design principle for the evolution of β-
889 lactamases from substrate promiscuity to specificity. *Nat. Commun.* 12:1852.

890 Moulana A, Dupic T, Phillips AM, Chang J, Nieves S, Roffler AA, Greaney AJ, Starr TN, Bloom JD, Desai
891 MM. 2022a. Compensatory epistasis maintains ACE2 affinity in SARS-CoV-2 Omicron BA.1. *Nat.*
892 *Commun.* 13:7011.

893 Moulana A, Dupic T, Phillips AM, Chang J, Nieves S, Roffler AA, Greaney AJ, Starr TN, Bloom JD, Desai
894 MM. 2022b. Compensatory epistasis maintains ACE2 affinity in SARS-CoV-2 Omicron BA.1. *Nat.*
895 *Commun.* 13:7011.

896 Moulana A, Dupic T, Phillips AM, Chang J, Roffler AA, Greaney AJ, Starr TN, Bloom JD, Desai MM. 2023.
897 The landscape of antibody binding affinity in SARS-CoV-2 Omicron BA.1 evolution. *eLife*
898 12:e83442.

899 Neher RA. 2022. Contributions of adaptation and purifying selection to SARS-CoV-2 evolution. *Virus Evol.*
900 8:veac113.

901 Nevin Gerek, Z., Kumar, S., Banu Ozkan, S. 2013. Structural dynamics flexibility informs function and
902 evolution at a proteome scale. *Evol Appl*.

903 Nguyen HL, Lan PD, Thai NQ, Nissley DA, O'Brien EP, Li MS. 2020. Does SARS-CoV-2 Bind to Human ACE2
904 More Strongly Than Does SARS-CoV? *J. Phys. Chem. B* 124:7336–7347.

905 Nielsen BF, Li Y, Sneppen K, Simonsen L, Viboud C, Levin SA, Grenfell BT. 2022. Immune Heterogeneity
906 and Epistasis Explain Punctuated Evolution of SARS-CoV-2. Epidemiology Available from:
907 http://medrxiv.org/lookup/doi/10.1101/2022.07.27.22278129

908 Nussinov, R., Tsai, C.-J. 2013. Allostery in disease and in drug discovery. *Cell* 153:293–305.

909 O'Rourke KF, Gorman SD, Boehr DD. 2016. Biophysical and computational methods to analyze amino
910 acid interaction networks in proteins. *Comput. Struct. Biotechnol. J.* 14:245–251.

911 Ose NJ, Butler BM, Kumar A, Kazan IC, Sanderford M, Kumar S, Ozkan SB. 2022. Dynamic coupling of
912 residues within proteins as a mechanistic foundation of many enigmatic pathogenic missense
913 variants.Wallqvist A, editor. *PLOS Comput. Biol.* 18:e1010006.

914 Ose NJ, Campitelli P, Patel RP, Ozkan SB, Kumar S. 2022. Protein dynamics provide mechanistic insights
915 about the epistatic relationships among highly observed potentially adaptive missense variants.
916 *Biophys. J.* 121:456a.

917 Otten R, Liu L, Kenner LR, Clarkson MW, Mavor D, Tawfik DS, Kern D, Fraser JS. 2018. Rescue of
918 conformational dynamics in enzyme catalysis by directed evolution. *Nat. Commun.* 9:1314.

919 Ozono S, Zhang Y, Ode H, Sano K, Tan TS, Imai K, Miyoshi K, Kishigami S, Ueno T, Iwatani Y, et al. 2021.
920 SARS-CoV-2 D614G spike mutation increases entry efficiency with enhanced ACE2-binding
921 affinity. *Nat. Commun.* 12:848.

922 Patel R, Scheinfeldt LB, Sanderford MD, Lanham TR, Tamura K, Platt A, Glicksberg BS, Xu K, Dudley JT,
923 Kumar S. 2018. Adaptive Landscape of Protein Variation in Human Exomes.Yeager M, editor.
924 *Mol. Biol. Evol.* 35:2015–2025.

925 de la Paz JA, Nartey CM, Yuvaraj M, Morcos F. 2020. Epistatic contributions promote the unification of
926 incompatible models of neutral molecular evolution. *Proc. Natl. Acad. Sci.* 117:5873–5882.

927 Pearlman DA, Case DA, Caldwell JW, Ross WS, Cheatham III TE, DeBolt S, Ferguson D, Seibel G, Kollman
928 P. 1995. AMBER, a package of computer programs for applying molecular mechanics, normal
929 mode analysis, molecular dynamics and free energy calculations to simulate the structural and
930 energetic properties of molecules. *Comput Phys Commun* 91:1–41.

931 Peters AD, Lively CM. 1999. The Red Queen and Fluctuating Epistasis: A Population Genetic Analysis of
932 Antagonistic Coevolution. *Am. Nat.* 154:393–405.

933 Pipitò L, Rujan R, Reynolds CA, Deganutti G. 2022. Molecular dynamics studies reveal structural and
934 functional features of the SARS-CoV-2 spike protein. *BioEssays* 44:2200060.

935 Qu P, Faraone JN, Evans JP, Zheng Y-M, Carlin C, Anghelina M, Stevens P, Fernandez S, Jones D, Panchal
936 A, et al. 2023. Extraordinary Evasion of Neutralizing Antibody Response by Omicron XBB.1.5,
937 CH.1.1 and CA.3.1 Variants. Microbiology Available from:
938 http://biorxiv.org/lookup/doi/10.1101/2023.01.16.524244

939 Raghuvamsi PV, Tulsian NK, Samsudin F, Qian X, Purushotorman K, Yue G, Kozma MM, Hwa WY, Lescar J,
940 Bond PJ, et al. 2021. SARS-CoV-2 S protein:ACE2 interaction reveals novel allosteric targets. *eLife*
941 10:e63646.

942 Ramarao-Milne P, Jain Y, Sng LMF, Hosking B, Lee C, Bayat A, Kuiper M, Wilson LOW, Twine NA, Bauer
943 DC. 2022. Data-driven platform for identifying variants of interest in COVID-19 virus. *Comput.*
944 *Struct. Biotechnol. J.* 20:2942–2950.

945 Rehman S ur, Shafique L, Ihsan A, Liu Q. 2020. Evolutionary Trajectory for the Emergence of Novel
946 Coronavirus SARS-CoV-2. *Pathogens* 9:240.

947 Rizzato F, Coucke A, de Leonardis E, Barton JP, Tubiana J, Monasson R, Cocco S. 2020. Inference of
948 compressed Potts graphical models. *Phys. Rev. E* 101:012309.

949 Rochman ND, Faure G, Wolf YI, Freddolino PL, Zhang F, Koonin EV. 2022. Epistasis at the SARS-CoV-2
950 Receptor-Binding Domain Interface and the Propitiously Boring Implications for Vaccine
951 Escape.Diamond MS, editor. *mBio* 13:e00135-22.

952 Rochman ND, Wolf YI, Faure G, Mutz P, Zhang F, Koonin EV. 2021. Ongoing global and regional adaptive
953 evolution of SARS-CoV-2. *Proc. Natl. Acad. Sci.* 118:e2104241118.

954 Rodriguez-Rivas J, Croce G, Muscat M, Weigt M. 2022. Epistatic models predict mutable sites in SARS-
955 CoV-2 proteins and epitopes. *Proc. Natl. Acad. Sci.* 119:e2113118119.

956 Rojas Echenique JI, Kryazhimskiy S, Nguyen Ba AN, Desai MM. 2019. Modular epistasis and the
957 compensatory evolution of gene deletion mutants.Butler G, editor. *PLOS Genet.* 15:e1007958.

958 Saavedra HG, Wrabl JO, Anderson JA, Li J, Hilser VJ. 2018. Dynamic allostery can drive cold adaptation in
959 enzymes. *Nature* 558:324–328.

960 Saputri DS, Li S, van Eerden FJ, Rozewicki J, Xu Z, Ismanto HS, Davila A, Teraguchi S, Katoh K, Standley
961 DM. 2020. Flexible, Functional, and Familiar: Characteristics of SARS-CoV-2 Spike Protein
962 Evolution. *Front. Microbiol.* 11:2112.

963 Sawle L, Ghosh K. 2016. Convergence of Molecular Dynamics Simulation of Protein Native States:
964 Feasibility vs Self-Consistency Dilemma. *J. Chem. Theory Comput.* 12:861–869.

965 Sekhar A, Kay LE. 2019. An NMR View of Protein Dynamics in Health and Disease. *Annu. Rev. Biophys.*
966 48:297–319.

967 Shang J, Wan Y, Luo C, Ye G, Geng Q, Auerbach A, Li F. 2020. Cell entry mechanisms of SARS-CoV-2. *Proc.*
968 *Natl. Acad. Sci.* 117:11727–11734.

969 Shimagaki K, Weigt M. 2019. Selection of sequence motifs and generative Hopfield-Potts models for
970 protein families. *Phys. Rev. E* 100:032128.

971 Shoemark DK, Oliveira ASF, Davidson AD, Berger I, Schaffitzel C, Mulholland AJ. 2022. Molecular
972 dynamics of spike variants in the locked conformation: RBD interfaces, fatty acid binding and

furin cleavage sites. Biochemistry Available from: http://biorxiv.org/lookup/doi/10.1101/2022.05.06.490927

Singh D, Yi SV. 2021. On the origin and evolution of SARS-CoV-2. *Exp. Mol. Med.* 53:537–547.

Socher E, Conrad M, Heger L, Paulsen F, Sticht H, Zunke F, Arnold P. 2021. Mutations in the B.1.1.7 SARS-CoV-2 Spike Protein Reduce Receptor-Binding Affinity and Induce a Flexible Link to the Fusion Peptide. *Biomedicines* 9:525.

Spinello A, Saltalamacchia A, Borišek J, Magistrato A. 2021. Allosteric Cross-Talk among Spike's Receptor-Binding Domain Mutations of the SARS-CoV-2 South African Variant Triggers an Effective Hijacking of Human Cell Receptor. *J. Phys. Chem. Lett.* 12:5987–5993.

Starr TN, Greaney AJ, Hannon WW, Loes AN, Hauser K, Dillen JR, Ferri E, Farrell AG, Dadonaite B, McCallum M, et al. 2022. Shifting mutational constraints in the SARS-CoV-2 receptor-binding domain during viral evolution. *Science* 377:420–424.

Starr TN, Greaney AJ, Stewart CM, Walls AC, Hannon WW, Veesler D, Bloom JD. 2022. Deep mutational scans for ACE2 binding, RBD expression, and antibody escape in the SARS-CoV-2 Omicron BA.1 and BA.2 receptor-binding domains.Mok CKP, editor. *PLOS Pathog.* 18:e1010951.

Starr TN, Zepeda SK, Walls AC, Greaney AJ, Alkhovsky S, Veesler D, Bloom JD. 2022. ACE2 binding is an ancestral and evolvable trait of sarbecoviruses. *Nature* 603:913–918.

Steinhauer DA. 1999. Role of Hemagglutinin Cleavage for the Pathogenicity of Influenza Virus. *Virology* 258:1–20.

Stevens AO, Kazan IC, Ozkan B, He Y. 2022. Investigating the allosteric response of the PICK1 PDZ domain to different ligands with all-atom simulations. *Protein Sci.* 31:e4474.

Sun PA Y, Kollman. 1995. Hydrophobic solvation of methane and nonbond parameters of the TIP3P water model. *J Comput Chem* 16:1164–1169.

Swint-Kruse L, Matthews KS, Smith PE, Pettitt BM. 1998. Comparison of Simulated and Experimentally Determined Dynamics for a Variant of the LacI DNA-Binding Domain, Nlac-P. *Biophys. J.* 74:413–421.

Sztain T, Ahn S-H, Bogetti AT, Casalino L, Goldsmith JA, Seitz E, McCool RS, Kearns FL, Acosta-Reyes F, Maji S, et al. 2021. A glycan gate controls opening of the SARS-CoV-2 spike protein. *Nat. Chem.* 13:963–968.

Tan ZW, Tee W-V, Samsudin F, Guarnera E, Bond PJ, Berezovsky IN. 2022. Allosteric perspective on the mutability and druggability of the SARS-CoV-2 Spike protein. *Structure* 30:590-607.e4.

Tang X, Wu C, Li X, Song Y, Yao X, Wu X, Duan Y, Zhang H, Wang Y, Qian Z, et al. 2020. On the origin and continuing evolution of SARS-CoV-2. *Natl. Sci. Rev.* 7:1012–1023.

Tay JH, Porter AF, Wirth W, Duchene S. 2022. The Emergence of SARS-CoV-2 Variants of Concern Is Driven by Acceleration of the Substitution Rate.Leitner T, editor. *Mol. Biol. Evol.* 39:msac013.

1008 Teruel Natalia, Crown M, Bashton M, Najmanovich R. 2021. Computational analysis of the effect of
1009 SARS-CoV-2 variant Omicron Spike protein mutations on dynamics, ACE2 binding and propensity
1010 for immune escape. Biophysics Available from:
1011 http://biorxiv.org/lookup/doi/10.1101/2021.12.14.472622

1012 Teruel Natália, Mailhot O, Najmanovich RJ. 2021a. Modelling conformational state dynamics and its role
1013 on infection for SARS-CoV-2 Spike protein variants.Dunbrack RL, editor. *PLOS Comput. Biol.*
1014 17:e1009286.

1015 Teruel Natália, Mailhot O, Najmanovich RJ. 2021b. Modelling conformational state dynamics and its role
1016 on infection for SARS-CoV-2 Spike protein variants.Dunbrack RL, editor. *PLOS Comput. Biol.*
1017 17:e1009286.

1018 Thye AY-K, Law JW-F, Pusparajah P, Letchumanan V, Chan K-G, Lee L-H. 2021. Emerging SARS-CoV-2
1019 Variants of Concern (VOCs): An Impending Global Crisis. *Biomedicines* 9:1303.

1020 Verkhivker G. 2022. Allosteric Determinants of the SARS-CoV-2 Spike Protein Binding with Nanobodies:
1021 Examining Mechanisms of Mutational Escape and Sensitivity of the Omicron Variant. *Int. J. Mol.*
1022 *Sci.* 23:2172.

1023 Walls AC, Park Y-J, Tortorici MA, Wall A, McGuire AT, Veesler D. 2020. Structure, Function, and
1024 Antigenicity of the SARS-CoV-2 Spike Glycoprotein. *Cell* 181:281-292.e6.

1025 Wang Q, Guo Y, Iketani S, Nair MS, Li Z, Mohri H, Wang M, Yu J, Bowen AD, Chang JY, et al. 2022.
1026 Antibody evasion by SARS-CoV-2 Omicron subvariants BA.2.12.1, BA.4 and BA.5. *Nature*
1027 608:603–608.

1028 Wang Q, Iketani S, Li Z, Liu Liyuan, Guo Y, Huang Y, Bowen AD, Liu M, Wang M, Yu J, et al. 2022. Alarming
1029 antibody evasion properties of rising SARS-CoV-2 BQ and XBB subvariants.
1030 *Cell*:S0092867422015318.

1031 Weisblum Y, Schmidt F, Zhang F, DaSilva J, Poston D, Lorenzi JC, Muecksch F, Rutkowska M, Hoffmann H-
1032 H, Michailidis E, et al. 2020. Escape from neutralizing antibodies by SARS-CoV-2 spike protein
1033 variants. *eLife* 9:e61312.

1034 Witte L, Baharani VA, Schmidt F, Wang Z, Cho A, Raspe R, Guzman-Cardozo C, Muecksch F, Canis M, Park
1035 DJ, et al. 2023. Epistasis lowers the genetic barrier to SARS-CoV-2 neutralizing antibody escape.
1036 *Nat. Commun.* 14:302.

1037 Wrapp D, Wang N, Corbett KS, Goldsmith JA, Hsieh C-L, Abiona O, Graham BS, McLellan JS. 2020. Cryo-
1038 EM structure of the 2019-nCoV spike in the prefusion conformation. *Science* 367:1260–1263.

1039 Wrobel AG, Benton DJ, Xu P, Roustan C, Martin SR, Rosenthal PB, Skehel JJ, Gamblin SJ. 2020. SARS-CoV-
1040 2 and bat RaTG13 spike glycoprotein structures inform on virus evolution and furin-cleavage
1041 effects. *Nat. Struct. Mol. Biol.* 27:763–767.

1042 Wu L, Zhou L, Mo M, Liu T, Wu C, Gong C, Lu K, Gong L, Zhu W, Xu Z. 2022. SARS-CoV-2 Omicron RBD
1043 shows weaker binding affinity than the currently dominant Delta variant to human ACE2. *Signal*
1044 *Transduct. Target. Ther.* 7:8.

1045 Xue Q, Liu X, Pan W, Zhang A, Fu J, Jiang G. 2022. Computational Insights into the Allosteric Effect and
1046 Dynamic Structural Features of the SARS-COV-2 Spike Protein. *Chem. – Eur. J.* [Internet] 28.
1047 Available from: https://onlinelibrary.wiley.com/doi/10.1002/chem.202104215

1048 Yang QE, MacLean C, Papkou A, Pritchard M, Powell L, Thomas D, Andrey DO, Li M, Spiller B, Yang W, et
1049 al. 2020. Compensatory mutations modulate the competitiveness and dynamics of plasmid-
1050 mediated colistin resistance in Escherichia coli clones. *ISME J.* 14:861–865.

1051 Yue C, Song W, Wang L, Jian F, Chen X, Gao F, Shen Z, Wang Y, Wang X, Cao Y. 2023. Enhanced
1052 transmissibility of XBB.1.5 is contributed by both strong ACE2 binding and antibody evasion.
1053 Immunology Available from: http://biorxiv.org/lookup/doi/10.1101/2023.01.03.522427

1054 Yurkovetskiy L, Wang X, Pascal KE, Tomkins-Tinch C, Nyalile TP, Wang Y, Baum A, Diehl WE, Dauphin A,
1055 Carbone C, et al. 2020. Structural and Functional Analysis of the D614G SARS-CoV-2 Spike
1056 Protein Variant. *Cell* 183:739-751.e8.

1057 Zeng H-L, Dichio V, Rodríguez Horta E, Thorell K, Aurell E. 2020. Global analysis of more than 50,000
1058 SARS-CoV-2 genomes reveals epistasis between eight viral genes. *Proc. Natl. Acad. Sci.*
1059 117:31519–31526.

1060 Zhang J, Cai Y, Xiao T, Lu J, Peng H, Sterling SM, Walsh RM, Rits-Volloch S, Zhu H, Woosley AN, et al.
1061 2021. Structural impact on SARS-CoV-2 spike protein by D614G substitution. *Science* 372:525–
1062 530.

1063 Zhou T, Tsybovsky Y, Gorman J, Rapp M, Cerutti G, Chuang G-Y, Katsamba PS, Sampson JM, Schön A,
1064 Bimela J, et al. 2020. Cryo-EM Structures of SARS-CoV-2 Spike without and with ACE2 Reveal a
1065 pH-Dependent Switch to Mediate Endosomal Positioning of Receptor-Binding Domains. *Cell Host*
1066 *Microbe* 28:867-879.e5.

1067

1068

1069 **<u>Supplemental Figures</u>**

	18	19	20	26	27	67	80	83	95	138	142	145	146	158	183	190	212	213	215	252	339	346	368	371	373	375	376	405	408	417	440	445
Wild-type (MN90894.3)	L	T	T	P	A	A	D	V	T	D	G	Y	H	R	Q	R	L	V	D	G	G	R	L	S	S	S	T	D	R	K	N	V
Alpha	L	T	T	P	A	A	D	V	T	D	G	Y	H	R	Q	R	L	V	D	G	G	R	L	S	S	S	T	D	R	K	N	V
Beta	L	T	T	P	A	A	A	V	T	D	G	Y	H	R	Q	R	L	V	G	G	G	R	L	S	S	S	T	D	R	N	N	V
Gamma	F	T	N	S	A	A	D	V	T	Y	G	Y	H	R	Q	S	L	V	D	G	G	R	L	S	S	S	T	D	R	T	N	V
Delta	L	R	T	P	A	A	D	V	T	D	G	Y	H	G	Q	R	L	V	D	G	G	R	L	S	S	S	T	D	R	K	N	V
Omicron	L	T	T	P	A	V	D	V	I	D	G	D	H	R	Q	R	I	V	D	G	D	R	L	L	P	F	T	D	R	N	K	V
Omicron XBB 1.5	L	I	T	P	S	A	D	A	T	D	D	Y	Q	R	E	R	L	E	D	V	H	T	I	F	P	F	A	N	S	N	K	P

	446	452	460	477	478	484	486	490	493	496	498	501	505	547	570	614	655	679	681	701	716	764	796	856	950	954	969	981	982	1027	1118	1176
Wild-type (MN90894.3)	G	L	N	S	T	E	F	F	Q	G	Q	N	Y	T	A	D	H	N	P	A	T	N	D	N	D	Q	N	L	S	T	D	V
Alpha	G	L	N	S	T	E	F	F	Q	G	Q	Y	Y	T	D	G	H	N	H	A	I	N	D	N	D	Q	N	L	A	T	H	V
Beta	G	L	N	S	T	K	F	F	Q	G	Q	Y	Y	T	A	G	H	N	P	V	T	N	D	N	D	Q	N	L	S	T	D	V
Gamma	G	L	N	S	T	K	F	F	Q	G	Q	Y	Y	T	A	G	Y	N	P	A	T	N	D	N	D	Q	N	L	S	I	D	F
Delta	G	R	N	S	K	E	F	F	Q	G	Q	N	Y	T	A	G	H	N	R	A	T	N	D	N	N	Q	N	L	S	T	D	V
Omicron	S	L	N	N	K	A	F	F	R	S	R	Y	H	K	A	G	Y	K	H	A	T	K	Y	K	D	H	K	F	S	T	D	V
Omicron XBB 1.5	S	L	K	N	K	A	P	S	Q	G	R	Y	H	T	A	G	Y	K	H	A	T	K	Y	N	D	H	K	L	S	T	D	V

Supplementary figure S1. A comparison of the amino acid sequences for different variant spike proteins used in this paper. Sequence MN90894.3 is used as the wild-type (reference) sequence. For each different variant, residue positions matching the reference sequence are shown in blue, while locations where the residue differs from the reference sequence are shown in yellow. For S protein locations not shown here, all variants presented have the same amino acid type as the reference sequence.

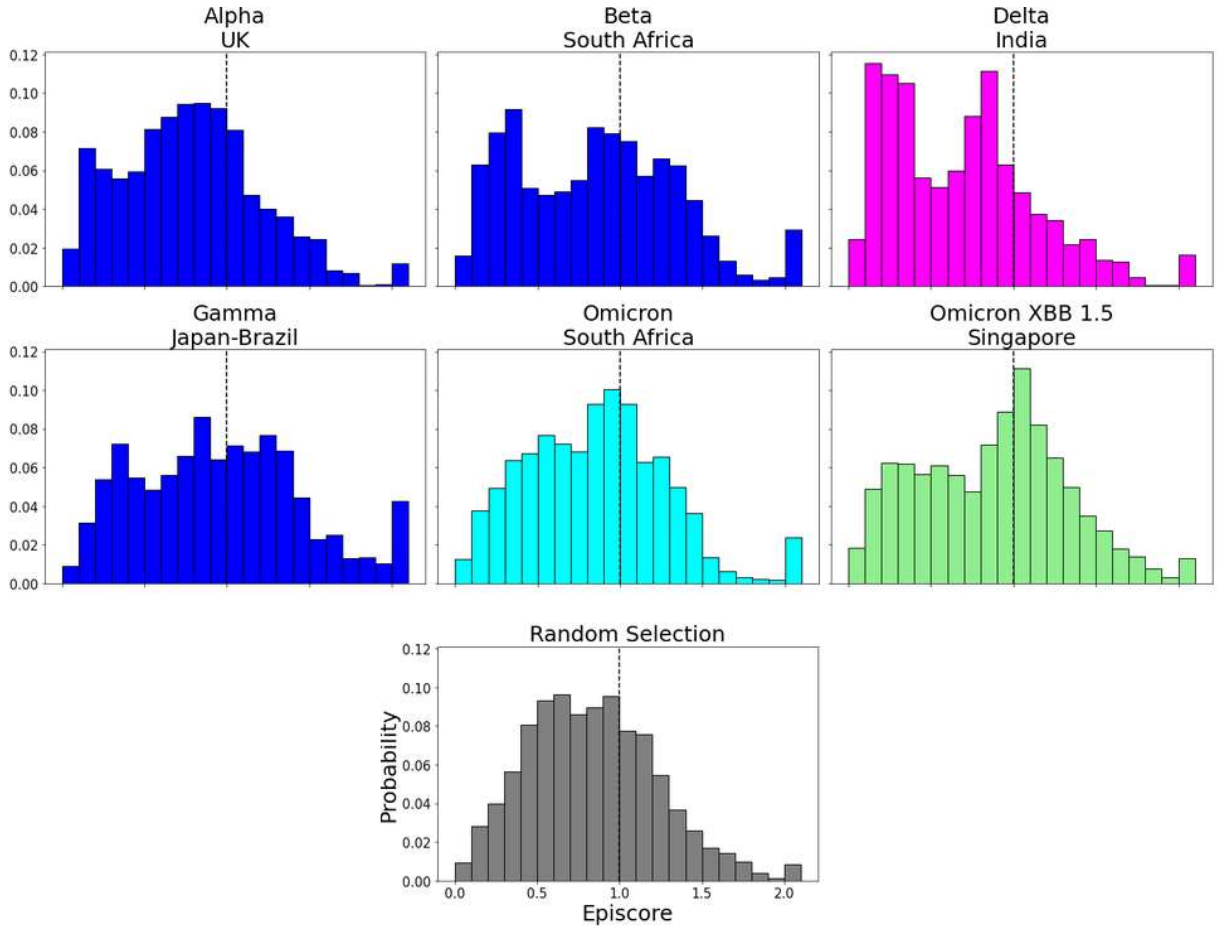

Supplementary figure S2. EpiScores with i = characteristic mutation sites, j = low EP sites, and k = the binding interface of the open chain. EpiScores using variant sites are significantly different ($p<.001$) from a set of EpiScores using random sites.

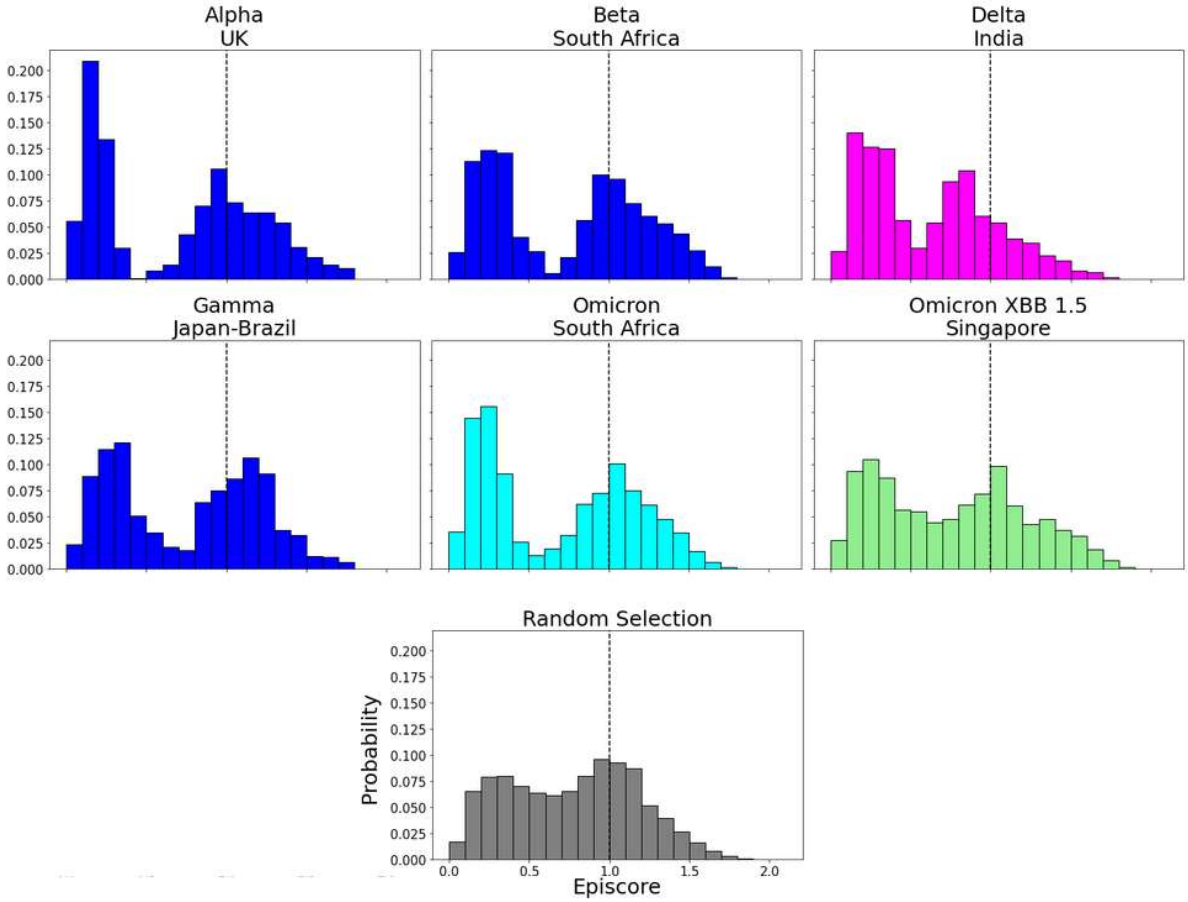

Supplementary figure S3. EpiScores with i = characteristic mutation sites within the NTD, j = low EP sites, and k = the binding interface of the open chain. NTD domain mutation sites result in markedly lower EpiScores compared to elsewhere.

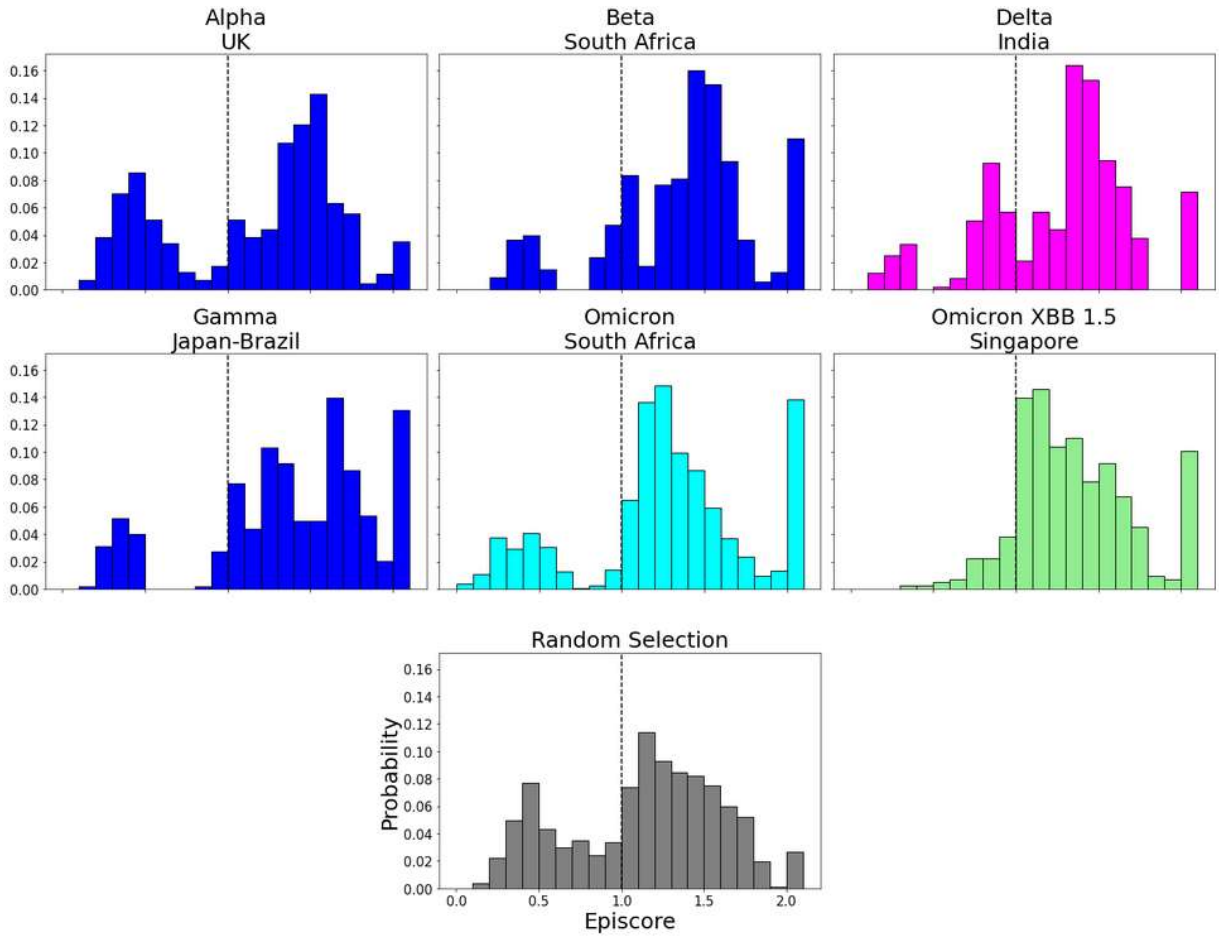

Supplementary figure S4. EpiScores with i = characteristic mutation sites, j = site 486, and k = the binding interface of the open chain. CAP and hACE2 and antibody binding site 486 displays epistasis with almost all XBB 1.5 variant sites at almost every hACE2 binding site. EpiScores using variant sites are significantly different ($p<.001$) from a set of EpiScores using random sites.

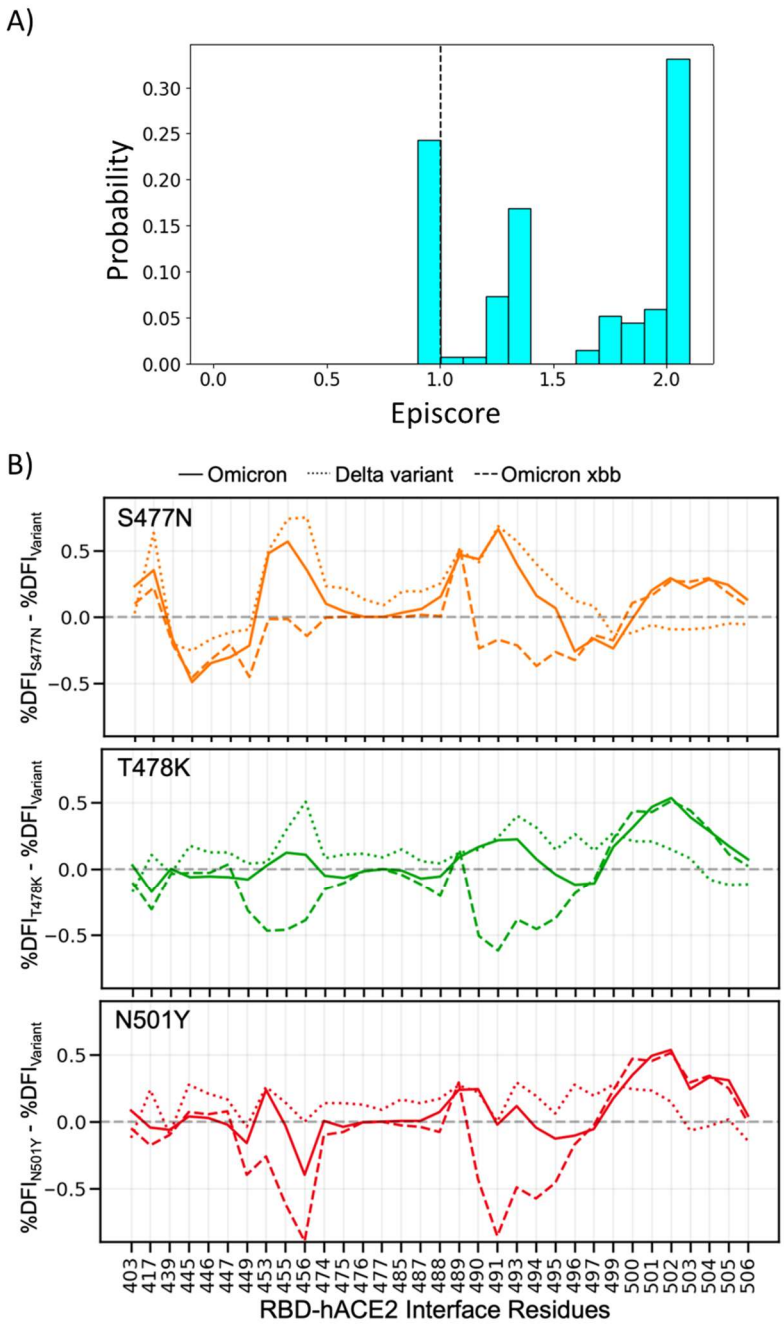

Supplementary figure S5. (A) Three critical mutations that emerged quickly, and were frequently observed in other dominant variants are S477N, T478K, and N501Y. EpiScores of sites 477, 478, and 501 with one another are shown (with k = the binding interface of the open chain). These residues are highly epistatic, producing higher responses than expected when perturbed together. (B) The difference in the dynamic flexibility profiles between the single mutants and

1100 the most common variants for the hACE2 binding residues of the RBD. The DFI profiles exhibit
1101 significantly different flexibility in each background variant, highlighting the critical non-additive
1102 interactions of the other mutation in the given background variant. Thus, these three binding
1103 affinity impacting mutations do not contribute only their own effects to the binding interface,
1104 there are epistatic interactions with the other mutations in VOCs that shape the dynamics of the
1105 binding interface to modulate binding.
1106
1107